Electron absorbed fractions of energy and S-values in an adult human skeleton based on μCT images of trabecular bone

R Kramer[1], R B Richardson[2], V F Cassola[1], J W Vieira[3, 4], H J Khoury[1], C A B de Oliveira Lira[1] and K Robson Brown[5]

[1] Department of Nuclear Energy, Federal University of Pernambuco, Avenida Prof. Luiz Freire, 1000, CEP 50740-540, Recife, Brazil

[2] Radiation Protection Research and Instrumentation Branch, Atomic Energy of Canada Limited, Chalk River Laboratories, Chalk River ON K0J 1J0, Canada

[3] Federal Institute of Education, Science and Technology of Pernambuco, Recife, Brazil

[4]Polytechnic School of Pernambuco, University of Pernambuco, Recife, Brazil

[5] Imaging Laboratory, Department of Archaeology and Anthropology, University of Bristol, Bristol, UK

E-mail: rkramer@uol.com.br

ABSTRACT

When the human body is exposed to ionizing radiation, among the soft tissues at risk are the active marrow (AM) and the bone endosteum (BE) located in tiny, irregular cavities of trabecular bone. Determination of absorbed fractions of energy or absorbed dose in the AM and the BE represent one of the major challenges of dosimetry. Recently, at the Department of Nuclear Energy at the Federal University of Pernambuco a skeletal dosimetry method based on μCT images of trabecular bone introduced into the spongiosa voxels of human phantoms has been developed and has been applied mainly to external exposure to photons. This study uses the same method to calculate absorbed fractions (AFs) of energy and S-values (absorbed dose per unit activity) for electron-emitting radionuclides known to concentrate in skeletal tissues. The modelling of the skeletal tissue regions follows ICRP110, which defines the BE as a 50 μm thick sub-region of marrow next to the bone surfaces. The paper presents mono-energetic AFs for the AM and the BE for eight different skeletal regions for electron source energies between 1 keV and 10 MeV. S-values are given for the beta-emitters ^{14}C, ^{59}Fe, ^{131}I, ^{89}Sr, ^{32}P and ^{90}Y. Comparisons with results from other investigations showed good agreement provided that differences between methodologies and trabecular bone volume fractions were properly taken into account. Additionally, a comparison was made between specific absorbed fractions (SAFs) of energy in the BE calculated for the actual 50 μm endosteum and the previously recommended 10 μm endosteum. The increase in endosteum thickness leads to a decrease of the endosteum absorbed dose by up to 3.7 fold when bone is the source region, while absorbed dose increases by ~20% when the beta-emitters are in marrow.

1. Introduction

There is general agreement that among the soft tissues located in the skeleton the haemopoietic and the stromal cells in the bone marrow, called active or red marrow, and the osteogenic precursor cells close to bone surfaces, called the bone endosteum, are most at risk with respect to radiation-induced leukemia and bone sarcoma, respectively. In the bones of the adult skeleton, the active marrow shares the cavities of trabecular bone mainly with fat cells, called inactive or yellow marrow, except for the lower long bones and the lower parts of the upper long bones, which contain only inactive marrow. The bone endosteum represents a layer of cells on all surfaces of trabecular bone, on interior surfaces of cortical bone next to trabecular bone or next to the inactive marrow in the medullary cavities of the long bones. In Publication 30, the International Commission on Radiological Protection (ICRP) recommended that for the active marrow, equivalent dose "is calculated as the average over the tissues which entirely fill the cavities within trabecular bone", while for the bone endosteum the equivalent dose "should be calculated as an average over tissue up to a distance of 10 μm from the relevant bone surfaces" (ICRP 1979).

Executing ICRP30's dosimetric proposal may become quite a challenging task because of the complex, irregular structure of the trabeculae and the marrow cavities, as figure 1 shows.

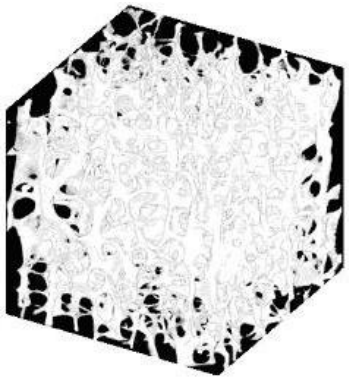

Figure1. 3D image (7.9 mm x 7.9 mm x 7.7 mm) of trabecular bone and marrow cavities. Extracted from μCT images of the 8. Thoracic vertebra scanned at 30 μm resolution (Kramer et al 2006b).

Pioneering work for the solution of this task has been done by Spiers and co-workers from the University of Leeds/UK, who, after some attempts based on stylized bone models (Spiers 1949, 1969), achieved a breakthrough in trabecular bone modeling with the determination of chord length distributions through trabeculae and cavities measured in human bone samples (Spiers 1974, Beddoe et al 1976, Whitwell and Spiers 1976). Based on chord length distributions and using Monte Carlo (MC) methods, Spiers and co-workers calculated dose rate factors for the active marrow and for the 10 μm bone endosteum for bone-seeking radionuclides, using the composition for muscle for all soft tissues in the trabecular cavities (Spiers et al 1978, 1981, Spiers 1988). The Leeds group also determined marrow rad/R and dose enhancement conversion factors for external photon irradiation (Spiers 1963, 1968, King and Spiers 1985), which were used by others for the calculation of active marrow equivalent or absorbed dose conversion coefficients for external exposure (Rosenstein 1976, Kramer 1979, Schlattl et al 2007).

The relative amount of active marrow in each bone is expressed by the cellularity factor (CF), which is the volume ratio between active and total marrow. With the publication of age-dependent, bone-specific CFs (Cristy 1981) it became possible to calculate the active marrow equivalent dose by multiplying the energy deposited in the total marrow by the corresponding CF and dividing the result by the active marrow mass, based on the assumption of a homogeneous distribution of active marrow in the trabecular cavities. This method and the chord length distributions of the Leeds group were

used by Eckerman and co-workers from the Oak Ridge National Laboratory (ORNL) for the calculation of absorbed fractions of energy in the active marrow and the bone endosteum from electron sources located in bone as well as in marrow and also of fluence-to-dose response functions for external exposure to photons (Eckerman 1985, Cristy and Eckerman 1987, Eckerman and Stabin 2000). Results from these studies were used in the MIRDOSE software for internal dosimetry (Stabin 1996).

Initially, skeletal dosimetry at the University of Florida (UF) was also based on the chord length distributions of the Leeds group (Bouchet et al 1999, 2000), but soon this method was replaced by a new concept of trabecular bone modelling based on μCT images of human bone samples which allows for particle transport through a three dimensional trabecular microstructure including segmented active and inactive marrow regions in the marrow cavities. Calculations of absorbed fractions of energy for active marrow and the bone endosteum from electron sources in trabecular bone and marrow for selected bone sites were performed with a MC code, which became known as Paired-Image Radiation Transport (PIRT) code (Jokisch et al 2001, Bolch et al 2002, Shah et al 2005a, b).

The effect of trabecular bone remodeling on absorbed fractions of energy and absorbed dose in active marrow and the bone endosteum was studied by Richardson and co-workers based on stylized trabecular bone models (Richardson and Dubeau 2003, Richardson et al 2007, Nie and Richardson 2009). They found significant differences in the absorbed fractions for two types of bone surface, quiescent and forming.

In 2009, the ICRP released Publication 110 on the Adult Reference Computational Phantoms which states: "A sub-region of the bone marrow, 50 μm from the bone surface, is further defined as the endosteal tissues" (ICRP 2009). The thickness of the bone endosteum was raised from 10 to 50 μm based on recent radiobiological findings with respect to the location of the cells relevant for radiation-induced bone cancer. For skeletal dosimetry it is important to note that according to ICRP30 and ICRP110, the bone marrow tissues "entirely fill the cavities within trabecular bone" (ICRP 1979) and the bone endosteum is a "sub-region of the bone marrow" (ICRP 2009).

Until 2006, the computational dosimetry group of the Department of Nuclear Energy at the Federal University of Pernambuco (UFPE) developed human phantoms with homogeneous skeletons, i.e. all bones were composed of a homogeneous mixture of bone and marrow. Equivalent doses to active marrow and the bone endosteum from external exposure to photons were calculated (Kramer et al 2003, 2004) based on marrow dose enhancement factors (King and Spiers 1985) and CFs (Cristy 1981) or using fluence-to-dose response functions (Cristy and Eckerman 1987). Starting in 2006, the transformation of skeletal dosimetry to the application of μCT images of trabecular bone in the whole skeleton was done in four steps: First, the homogeneous skeletons of the human male and female phantoms were segmented into cortical bone, spongiosa (= trabecular bone plus the soft tissues in the cavities), inactive marrow in the medullary cavities of the long bones and cartilage (Kramer et al 2006a). Second, trabecular microstructure was extracted from 3D μCT images of human bone samples, segmented into marrow cavities and bone trabeculae and introduced into the spongiosa voxels of the skeletons (Kramer et al 2006b). Third, an algorithm was developed to define a 10 or a 50 μm layer for the bone endosteum at runtime in all marrow micro voxels neighbouring trabecular and cortical bone (Kramer et al 2007, 2009a). Finally, an algorithm was developed to segment active and inactive marrow in the trabecular cavities at runtime based on CFs defined by the user (Kramer et al 2009b, 2010)

In the past, the UFPE model of skeletal dosimetry was used for external exposure. The purpose of this study is to apply the method to beta-emitters which are known to concentrate in various skeletal tissues, and to calculate absorbed and specific absorbed fractions of energy and S-values for the active marrow and the 50 μm bone endosteum in the skeleton of an adult male assuming quiescent bone surfaces.

2. Materials and methods

2.1 The exposure model

The exposure model used for this study consisted of the MASH2 standing phantom and 3D μCT images of trabecular bone connected to the EGSnrc MC code (Kawrakow and Rogers 2003) for the purpose of coupled transport of photons and electrons. The development of the phantom and the method of skeletal dosimetry have been reported earlier (Kramer et al 2010). Therefore, a summary of the exposure model is given here.

2.1.1 The MASH2 phantom

MASH2 (Cassola et al 2010b) is the updated version of the MASH (Male Adult meSH) phantom (Cassola et al 2010a), which was developed by modeling organs and tissues based on anatomical atlases using polygon mesh surfaces as well as 3D objects downloaded from the internet. The phantom has body mass, height, organ and tissue masses matched to reference data given by ICRP89 (ICRP 2002). The surface, the organs and the skeleton of the MASH2 phantom are shown in figures 2 and 3, respectively. The mesh phantom had to be voxelized in order to be connected to the EGSnrc MC code. Figure 4 depicts the voxelized version of the skeleton. Voxelization of the MASH2 phantom was done with cubic voxels of 1.2 mm x 1.2 mm x 1.2 mm, resulting in a matrix of 478 x 258 x 1462 = 180299688 macro voxel, 41776982 of which are filled with human tissue.

Figure 2. MASH2 skin

Figure 3. MASH2 organs/skeleton

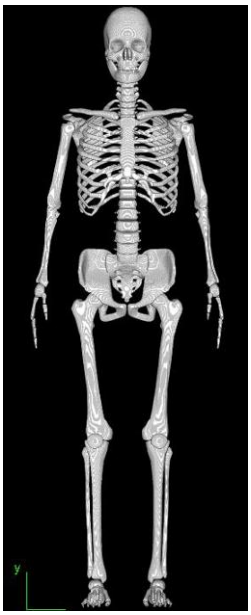

Figure 4. MASH2 voxelized skeleton

Figure 5a represents a transverse 2D image through the abdominal region of the MASH2 phantom exhibiting colon, small intestine, spine and pelvis. The close-up in figure 5b shows the spongiosa (brown) surrounded by cortical bone (green).

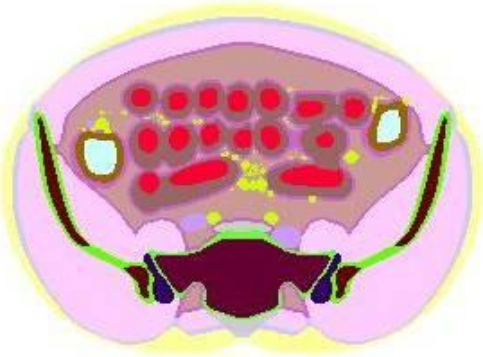

Figure 5a. MASH2 abdominal transverse image

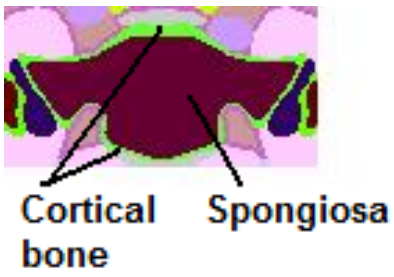

Figure 5b. MASH2 close-up spine/pelvis

2.1.2 The EGSnrc Monte Carlo code

Dosimetric data for this study were calculated with the EGSnrc MC code, version V4-2.3.1, released on February 19, 2010 and available at http://irs.inms.nrc.ca/software/egsnrc/. EGSnrc is one of the best bench-marked MC codes for coupled photon/electron transport with a dynamic range of charged particle kinetic energies between a few tens of keV and a few hundred GeV, and of photon energies between 1 keV and several hundred GeV. All EGSnrc transport parameters and cross section options were left at their default values, which are set to achieve the best accuracy EGSnrc is capable of.

2.1.3 The 8 SP cluster method for skeletal dosimetry

The description of the 8 SP cluster method is based on a recently published paper (Kramer et al 2010), but will present some additional information, like the skeletal tissue distribution in the MASH2 phantom and the segmentation scheme.

2.1.3.1 Segmentation of skeletal tissues

Based on data taken from ICRP Publications (ICRP 1995, 2002), the skeleton of the MASH2 voxel phantom has been segmented into cortical bone (1291637 voxel), spongiosa (2134502 voxel), medullary inactive marrow (349579 voxel) and cartilage (406421 voxel), with each voxel representing a 1.2 mm cube of the corresponding tissue. Next, human adult bone samples of the frontal bone (cranium), lumbar vertebra (L1), sternum, iliac crest (pelvis) and femur were extracted from a 30-year old female skeleton and were scanned at the Imaging Laboratory of the Department of Archaeology and Anthropology, University of Bristol, Bristol, UK at 60 μm resolution using a μCT scanner Skyscan 1172 (Skyscan Corporation, 2630 Aartselaar, Belgium) with 80 kV (100 μA). Then, the resulting 3D μCT images of spongiosa were segmented into trabecular bone and marrow cavity. After segmentation, the trabecular bone volume fractions, i.e. the fractions of bone in spongiosa were calculated as 11.4% for the sternum, 11.3% for the vertebra, 21.2% for the pelvis, 51.6% for the cranium and 15.2% for the femur which is in good agreement with corresponding data given by ICRP70 (ICRP 1995). 2.4 mm cubes of segmented spongiosa were extracted from each of the five 3D μCT images, with each cube representing a cluster of 2 x 2 x 2 = 8 micro matrices. Each micro matrix has the cubic dimensions of a spongiosa macro voxel, namely 1.2 mm, and contains 20 x 20 x 20 = 8000 micro voxels.

During execution, the MC code reads the MASH2 macro voxel matrix and then the five clusters, each of which contains 8 micro matrices, segmented into trabecular bone and marrow cavity. First, all cavity micro voxels were tagged as active marrow (AM) voxels. Then, based on CFs defined by the user, the MC code re-tags AM voxels into inactive marrow (IM) voxels, randomly distributed throughout the cavity volume, until the desired cellularity is achieved. Finally, the MC code segments the 50 μm bone endosteum in all marrow voxels neighboring bone voxels in spongiosa and in the medullary cavities of the long bones as described earlier (Kramer et al 2007, 2009a). For spongiosa, figure 6 shows a schematic 2D representation of trabecular bone (TB), active marrow (AM) and trabecular inactive marrow (IM) as a result of the segmentation process at runtime. The 50 μm bone endosteum corresponds to the area between trabecular bone and the broken line.

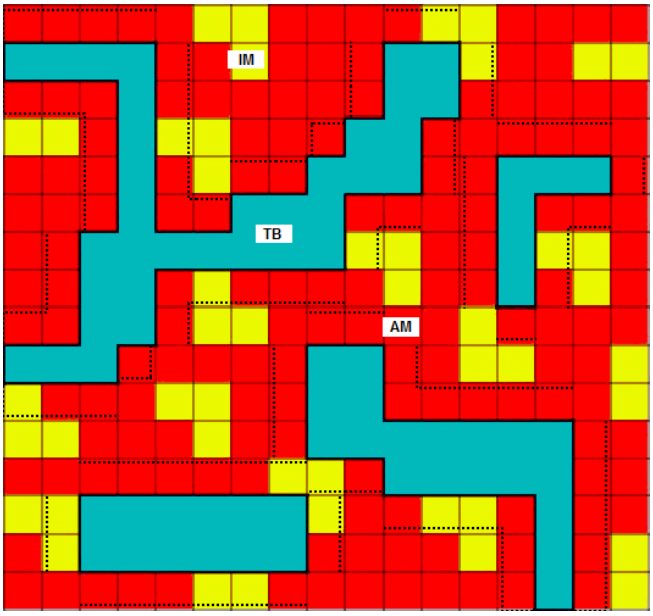

Figure 6. 2D schematic image of 60 μm pixels of trabecular bone (TB), active marrow (AM) and inactive marrow (IM) in spongiosa. The 50 μm bone endosteum is represented by the area between bone and the broken line.

The last step before particle transport starts is the calculation of the bone-specific volumes for trabecular bone, active marrow, inactive marrow and bone endosteum in all 2134502 spongiosa voxels based on the micro segmentation in the clusters. For the volume calculation, the 8 micro matrices in the clusters are used systematically and periodically (SP), i.e. they are not selected randomly but rather in a systematic sequential order and this sequence is repeated (periodically) as long as the next macro voxel is a spongiosa voxel. Additionally, the bone endosteum volume is also calculated in the medullary cavities filled with inactive marrow. The volumes for cortical bone, medullary inactive marrow and cartilage are calculated from the sums of their segmented macro voxels.

Table 1 shows the tissue volumes and masses in the MASH2 skeleton segmented with the method described above. Trabecular and medullary components are given for the bone endosteum and for the inactive marrow. ICRP reference masses are shown for comparison. With 5497.1 g, the total mineral bone mass of the MASH2 skeleton agrees with the ICRP89 mineral bone mass within a margin of 0.1%. However, the MASH2 masses of cortical and trabecular bone differ by 2.6% and 10.2%, respectively, from the reference masses. The active marrow mass of the MASH2 phantom is only 2.1% greater than the reference mass, while the inactive marrow mass is only 2.4% smaller. Cartilage masses differ significantly because the MASH2 skeleton contains only articular cartilage but

Table1. Tissue volumes, densities and masses in the MASH2 skeleton. Corresponding ICRP data are shown for comparison.

Male Adult		ICRP110	ICRP89	MASH2	MASH2	MASH2
		Mass	Mass	Volume	Density	Mass
Skeletal tissue	Acronym	(g)	(g)	(cm^3)	(g/cm^3)	(g)
Bone, cortical	CB		4400	2231.9	1.92	4285.2
Bone, trabecular	TB		1100	631.1	1.92	1211.9
Active marrow	AM		1170	1160.0	1.03	1194.8
Endosteum, trabecular	TBE			451.1	1.00	451.1
Endosteum, medullary	MBE			7.0	1.00	7.0
Endosteum, total	BE	544.4		458.1		458.1
Inactive marrow, trabecular	TIM			1860.0	0.98	1822.8
Inactive marrow, medullary	MIM			611.1	0.98	598.9
Inactive marrow, total	IM		2480	2471.1		2421.7
Cartilage			1100	686.6	1.10	755.3
Teeth			50	15.9	2.75	43.7
Miscellaneous			200			
Total skeleton			10500	7196.6	1.38	9912.6

no cartilage segmented outside the skeleton (nose, ears, etc.), while the ICRP reference mass includes all cartilage. The MASH2 bone endosteum mass is almost 16% smaller than the reference value given in ICRP110. ICRP110 refers to a paper of Bolch et al (2007), but unfortunately the authors did not provide enough information which could help to explain the disagreement. However, good agreement was found with data published by Watchman et al (2007), who used a completely different method for the calculation of skeletal tissue masses. Their calculated mass for "all bone marrow localized within 50 μm of the bone surfaces in spongiosa" was given as 434.6 g for the adult male, which differs from the 451.1 g shown table 1 by only 3.8%. In table1, the densities for bone, active marrow, inactive marrow and cartilage were taken from ICRU46 (ICRU 1992), the density for the teeth from ICRP110 (ICRP 2009) and the density for the bone endosteum was calculated as the volume-weighted average of the active and the inactive marrow densities in the trabecular cavities, because the bone endosteum is segmented in soft tissue micro voxels adjacent to bone, which can be either active or inactive marrow micro voxels as figure 6 shows. The density for the total skeleton is the ratio between total mass and total volume.

2.1.3.2 Calculation of energy deposited in active marrow and the bone endosteum

During radiation transport, every time a particle enters a spongiosa voxel the transport algorithm switches from the macro matrix (1.2 mm cubes) to the micro matrices containing 60 μm cubes of AM, TIM and TB and energy is deposited in the micro voxels of the skeletal tissues to be used for the calculation of absorbed fractions or doses. The application of the clusters in spongiosa during transport occurs systematically and periodically (SP) using the 8 micro matrices as described above. Tests with up to 8 x 8 x 8 = 512 micro matrices have shown that clusters with 2 x 2 x 2 = 8 micro matrices are sufficient to simulate adequately the trabecular microstructure in the spongiosa macro voxels for dosimetric purposes (Kramer et al 2009a). Therefore, this technique was called the 8 SP cluster method.

2.2 Target tissues, source regions and quantities of interest

For bone-seeking radionuclides in the adult skeleton the primary target tissues considered in this study are:

- AM The active marrow located in the spongiosa of all bones, except for the lower long bones and the lower parts of the upper long bones.
- BE The bone endosteum represented by the marrow located within a distance of 50 μm from all bone surfaces in spongiosa (TBE) and in the medullary cavities (MBE).

For electron-emitting bone-seekers, radiosensitive organs and tissues located outside the skeleton usually experience significantly lower absorbed fractions or doses than the AM or the BE due to the shielding effect by mineral bone and are therefore considered as secondary target tissues. However, for source energies above several MeV absorbed fractions or doses for secondary tissues begin to approach those for the skeletal tissues. Therefore, this study will show also some results for secondary target tissues.

It is assumed that radionuclides are uniformly distributed throughout a given source region and that beta-particles are isotropically emitted from every point within the source region. The source regions considered are:

- AM Active marrow (volume)
- TIM Trabecular inactive marrow (volume)
- TM Trabecular (active + inactive) marrow (volume)
- TBE Trabecular bone endosteum (volume)
- TBS Trabecular bone surface
- TBV Trabecular bone volume
- CBV Cortical bone volume
- CBS Cortical bone surface in the medullary cavities

The quantities to be determined for the whole skeleton are:

- AF (T←S, E) Absorbed fraction, defined as the fraction of radiation energy E emitted within the source tissue S that is absorbed in the target tissue T.

- SAF(T←S) Specific absorbed fraction, defined as the absorbed fraction AF (T←S, E) in target tissue T divided by the mass of target tissue T.

- S (T←S) Absorbed dose per unit activity, also called S-value, defined as the mean absorbed dose to target tissue T per nuclear transformation in source tissue S.

3. Results and discussion

3.1 Absorbed fractions for mono-energetic electron sources

Mono-energetic calculations of AFs for the whole skeleton have been performed for electrons with source energies between 1 keV and 10 MeV using cut-off energies of 2 keV for photons and 5 keV for electrons in all tissues. For electron source energies smaller than 10 keV the electron cut-off energy in skeletal tissues was 1keV. For the AFs of the primary target tissues AM and BE, the statistical error was below 0.3% for the source regions AM, TIM, TM , TBE and TBS, below 1.0% for source tissue TBV and between 5% and 0.2% for source tissue CBV. Absorbed fractions in medullary BE from electrons emitted on the CBS had statistical errors below 0.3%. AFs for secondary target tissues were included in figures and tables when the statistical error was less than 10%. In the calculations, the CFs, based on ICRP70 (ICRP 1995), were 0.6 for the ribcage (ribs, sternum, scapulae and clavicles), 0.7 for the spine (vertebrae and sacrum), 0.48 for the pelvis, 0.38 for the skull (cranium and mandible) and 0.25 for the long bones.

Table 2. Electron CSDA ranges in mineral bone and soft tissue from NIST data tables.

Electron Energy	CSDA Range (μm)	
(MeV)	Bone	Soft tissue
0.01	1.5	2.5
0.015	3.1	5.1
0.02	5.1	8.6
0.03	10.4	17.6
0.05	25.4	43.2
0.1	83.7	143.3
0.2	261.2	449.7
0.5	1166	1770
1	2530	4385
1.5	4092	7110
2	5651	9839
4	11672	20500
10	27990	50110
Density	1.92 g/cm^3	1.0 g/cm^3

For a given tissue environment, interpretation of data describing energy deposition by electrons is very much based on range considerations. Therefore, CSDA ranges in bone and soft tissue have been calculated with the NIST data tables (http://www.nist.gov/pml/data/radiation.cfm) and are shown in table 2 as a function of the electron energy. According to ICRP70, in spongiosa the mean widths of the bone trabeculae and of the marrow cavities are 257 μm and 1170 μm, respectively, i.e. that an electron needs a kinetic energy of about 200 keV to penetrate through a bone trabecula and about 400 keV to cross through a marrow cavity.

3.1.1 Primary target tissues

Absorbed fractions of energy in the AM and the BE of the MASH2 skeleton are shown in figures 7-10 and in tables 3-5. For each primary target tissue two figures are presented, one for the soft tissue source regions and one for the bone source regions. AFs(BE←CBS) are given in table 4.

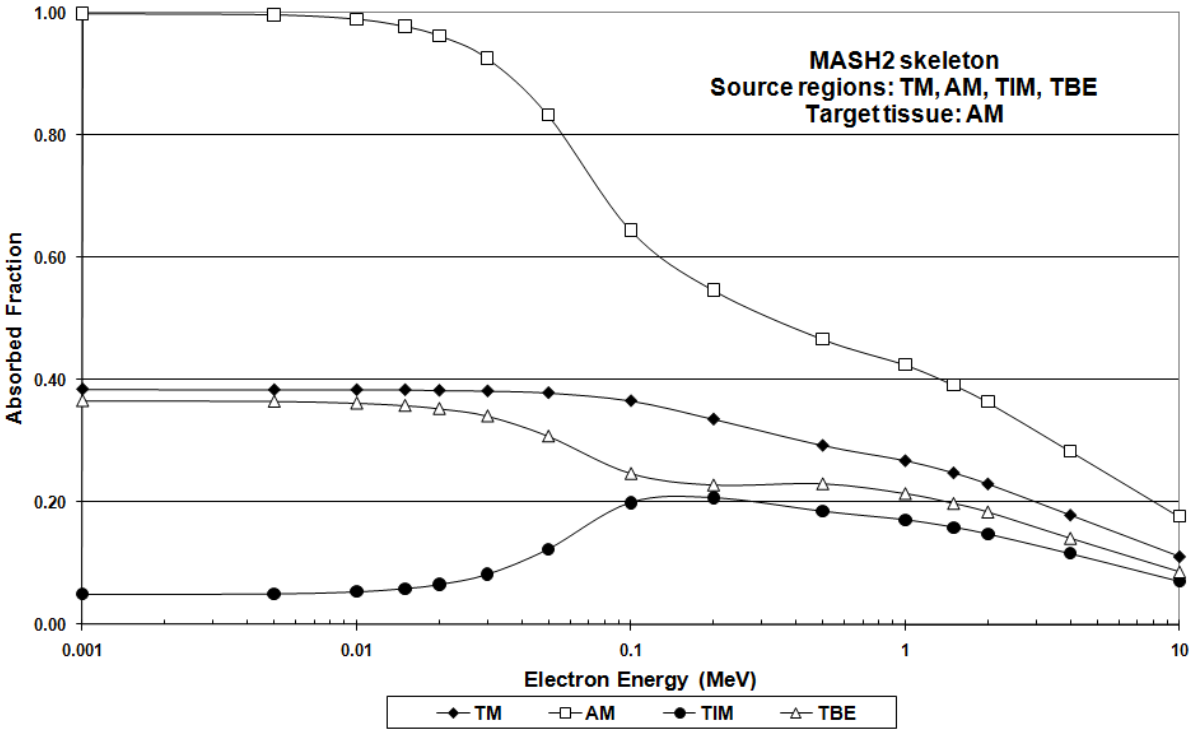

Figure 7a. Absorbed fractions of energy in the active marrow (AM) for electrons isotropically emitted in the trabecular marrow (TM), the active marrow (AM), the trabecular inactive marrow (TIM) and the trabecular bone endosteum (TBE) as a function of the electron source energy.

For soft tissue source regions T = AM, TIM, TM and TBE, figure 7a shows absorbed fractions of energy AF(AM←T) as a function of the source energy. When the AM is the source region and energies are below 20-30 keV, almost all emitted energy is absorbed in the AM, because, according to table 2, CSDA ranges in soft tissue are significantly smaller than the dimensions of the 60 μm voxels representing the skeletal tissues which are shown in figure 6. Consequently, the AF(AM←AM) is unity and starts to decrease significantly only for source energies above 20-30 keV, because with increasing energy more beta-particles can leave the AM micro voxels and deposit their energy first in neighboring TIM or TBV micro voxels and for higher energies also in the CBV or even in tissues located outside the skeleton. At 100 keV the AF(AM←AM) has decreased to 65%, at 1 MeV to 43% and at 10 MeV to 18%. For source region TIM, the AF(AM←TIM) starts with only 5% at 1 keV, because, apart from the small electron range, a significant amount of TIM is located in the lower long bones and the lower part of the upper long bones which do not contain AM. Then, the AF(AM←TIM) increases with energy and up to 30 keV it looks almost like a mirror curve of the AF(AM←AM). Absorption of energy in the AM increases until 200 keV to reach ca. 20%, but then starts decreasing with higher energies because of increasing absorption of energy first in TBV, then also in CBV and finally in tissues located outside the skeleton. Changing the CFs would quantitatively influence AF(AM←AM) and AF(AM←TIM), but would not change the character of the AF curves.

Source region TM reflects the case when the trabecular cavities are entirely filled with radionuclides, emitting electrons in AM and TIM voxels. The AF(AM←TM) is almost constant at around 38% up to 50 keV before it begins to decline for the reasons mentioned before for the AM and

the TIM sources. It does not come as a surprise that, at low energies, the AF(AM←TBE) is quite close to the AF(AM←TM), because the TBE is per definition a sub-volume of the marrow. What happens in the TM all over the cavity volume is essentially replicated within the TBE, although within the 50 μm thick sub-volume. For very small energies both, AF(AM←TBE) and AF(AM←TM) are almost equal. However, above 20-30 keV the spatial limits set by the 50 μm layer and the vicinity to the electron absorbing TBS become increasingly influential, and consequently the AF(AM←TBE) decreases more rapidly than the AF(AM←TM). Between 200 and 500keV the AF(AM←TBE) is constant at ca. 23%, while all other AFs decrease monotonously in this energy range. According to ICRP70, the mean width of the bone trabeculae in the adult skeleton is about 257 μm. Table 2 shows that an electron's energy has to be around 200 keV to cross through 261 μm of bone, i.e. that 200-500 keV beta-particles emitted from the TBE and crossing through trabeculae deposit more energy in the neighboring marrow cavity than electrons coming from locations deeper inside the marrow. Finally, the AF(AM←TBE) declines for the reasons mentioned already for the other AFs and reaches 9% at 10 MeV.

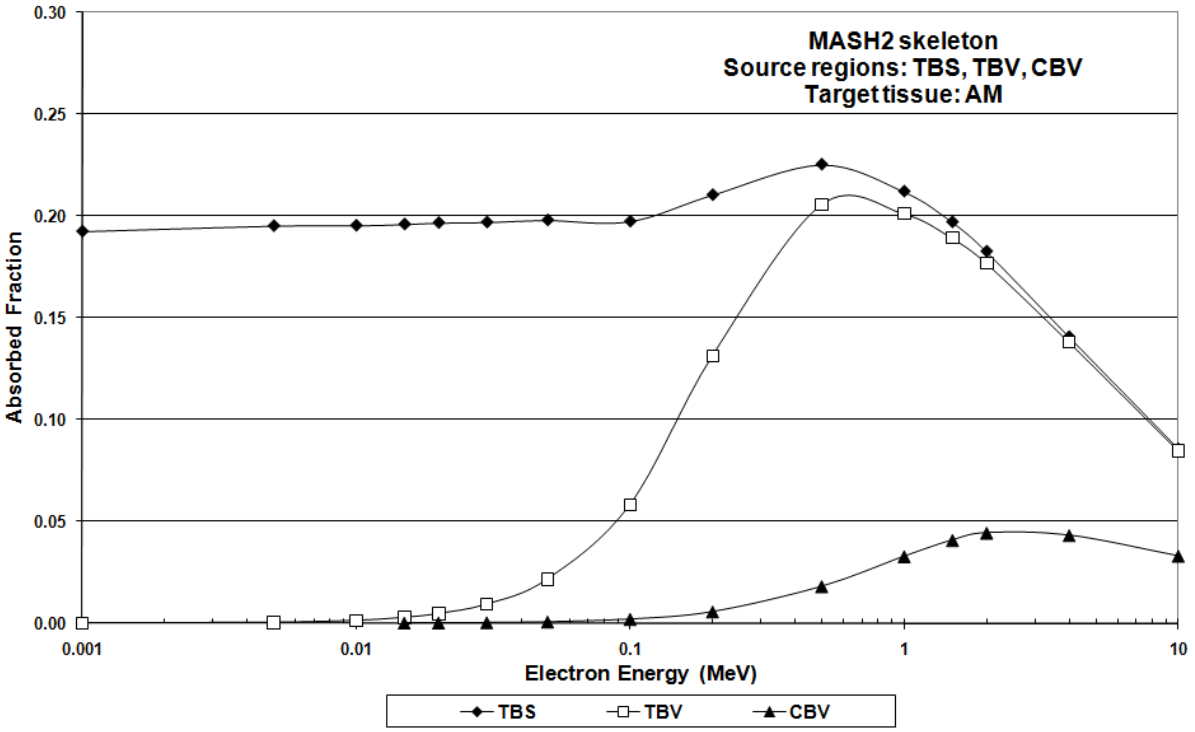

Figure 7b. Absorbed fractions of energy in the active marrow (AM) for electrons isotropically emitted on the trabecular bone surface (TBS), in the trabecular bone volume (TBV) and in the cortical bone volume (CBV) as a function of the electron source energy.

Figure 7b shows absorbed fractions for the AM when the source region is the bone surface or the bone volume. For electrons emitted on trabecular bone surfaces TBS, the AF(AM←TBS) is about 20% for energies up to 150 keV and this is mainly caused by those beta-particles emitted from the bone surface into the marrow cavity. As previously noted, as energies rise the electrons increasingly cross through the bone trabeculae and make an additional contribution to the absorbed fraction in the neighboring marrow cavity which leads to an increase of the AF(AM←TBS) up to 500 keV. For higher energies, electrons increasingly enter the CBV or leave the skeleton which causes a decline of the AF(AM←TBS) similar to those seen earlier for other AFs. The AF(AM←TBV) shows an energy dependence qualitatively similar to that of the AF(AM←TBS), but at much lower values for energies below 500 keV because, emitted inside the trabecular bone volume, electrons need much more energy to enter the marrow cavity and deposit energy in the AM. For higher energies both AFs become

increasingly similar and reach 9% at 10 MeV. Finally, when the cortical bone volume becomes the source region, only a few electrons reach the AM to deposit energy because of the shielding effect of mineral bone. Also many electrons are ejected out from the skeleton. Therefore, the AF(AM←CBV) is always very small and reaches a maximum of only 4.5% at 2 MeV.

Absorbed fractions of energy for the bone endosteum AF(BE←T) are shown in figure 8a for electrons emitted in soft tissue source regions T = AM, TIM, TM and TBE. When the TBE is the source region the energy dependence of the AF(BE←TBE) is similar to that seen above for the AF(AM←AM). Self-irradiation of tissue always causes this kind of curve. Yet, the AF(BE←TBE) declines faster with increasing energy due to the spatial confinement of the radionuclides to the 50 μm layer: 36% at 100 keV, 10% at 1 MeV and 1.3% at 10 MeV. The AFs for AM, TIM and TM source regions, being close together for all energies, change only moderately from 15% at 1 keV to 4% at 10 MeV. Up to about 50 keV, energy is deposited mainly by electrons emitted in AM, TIM or TM voxels within the 50 μm layer and the AFs are about 15%. For higher energies, endosteum electrons increasingly carry their energy beyond the 50 μm boundary, but at the same time electrons emitted in deeper marrow regions enter the endosteum, only partially compensating for the loss of energy, because the absorbed fractions decrease to about 10% at 100 keV. Further decrease of the AFs with energy is small in the region between 200 and 500 keV, where beta-particles have enough energy to cross through the bone trabeculae thereby causing additional deposition of energy in neighboring cavities. Finally, the AFs decline further towards 10 MeV to reach about 4%. Due to 100% TIM in the spongiosa of the lower long bones and the lower part of the upper long bones, the whole body AF(BE←TIM) is greater than the AF(BE←AM), but only by 0.5% to 1.0%.

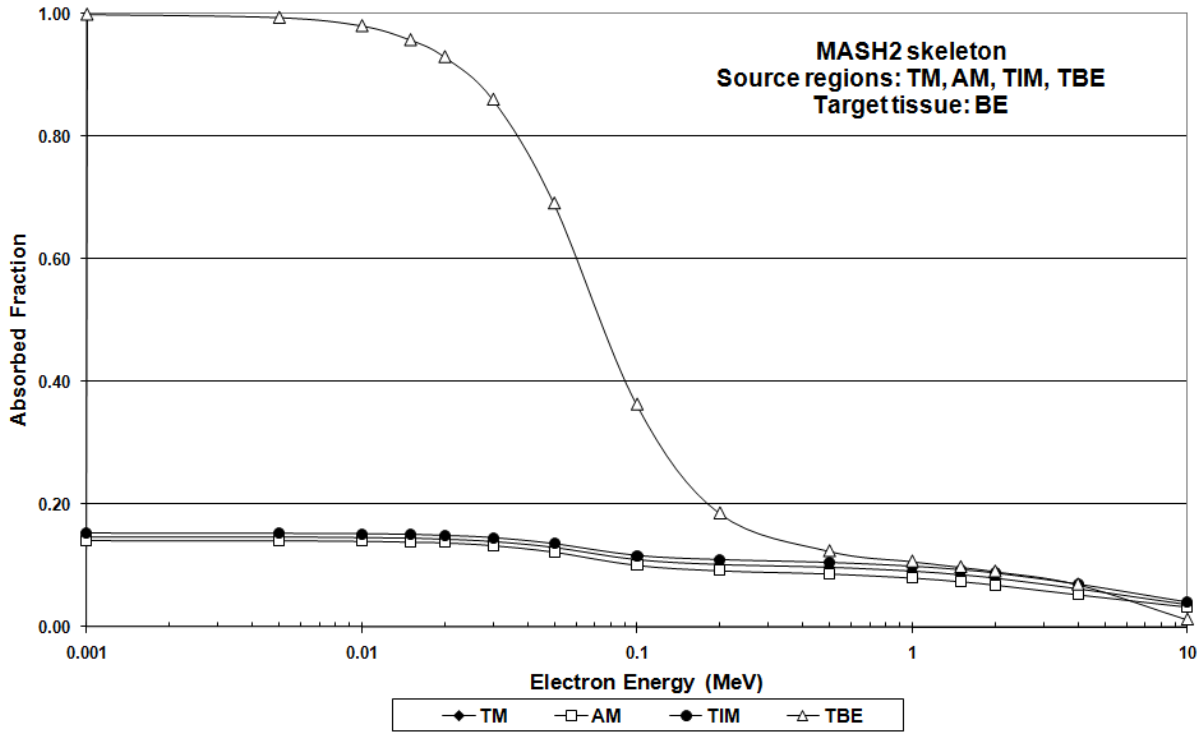

Figure 8a. Absorbed fractions of energy in the bone endosteum (BE) for electrons isotropically emitted in the active marrow (AM), the trabecular inactive marrow (TIM), the trabecular marrow (TM) and the trabecular bone endosteum (TBE) as a function of the electron source energy.

It seems reasonable to assume that all of the electrons emitted at the surface of trabecular bone (TBS) roughly 50% go into bone and the other half into the marrow cavity. With a value of slightly more than 50% between 1 and 50 keV, the AF(BE←TBS) in figure 8b reflects this

assumption. According to table 2, for energies greater than 50 keV the beta-particles travel beyond the 50 μm boundary and increasingly deposit their energy deeper in the marrow. Consequently, the AF(BE←TBS) starts to decline strongly from around 50 % at 50 keV down to about 17% at 200 keV and then at a slower rate down to 4% at 10 MeV. Again, the rate of decline changes typically between 200 and 500 keV when after penetration through trabeculae additional energy is deposited in neighbouring marrow cavities. But, this effect can only partially compensate for the energy loss to cortical bone, because all AFs continue to decrease for energies above 500 keV. The AFs for source regions TBV and CBV show basically the same pattern as seen before in figure 7b, however with much smaller values due to the spatial limitations of the target region to the 50 μm thickness. AF(BE←TBV) shows a maximum of 11% at 200 keV, while the greatest AF(BE←CBV) is 2% at 2-4 MeV. All absorbed fractions AF(AM←T) and AF(BE←T) shown in figures 7a to 8b are also presented in tables 3 and 4.

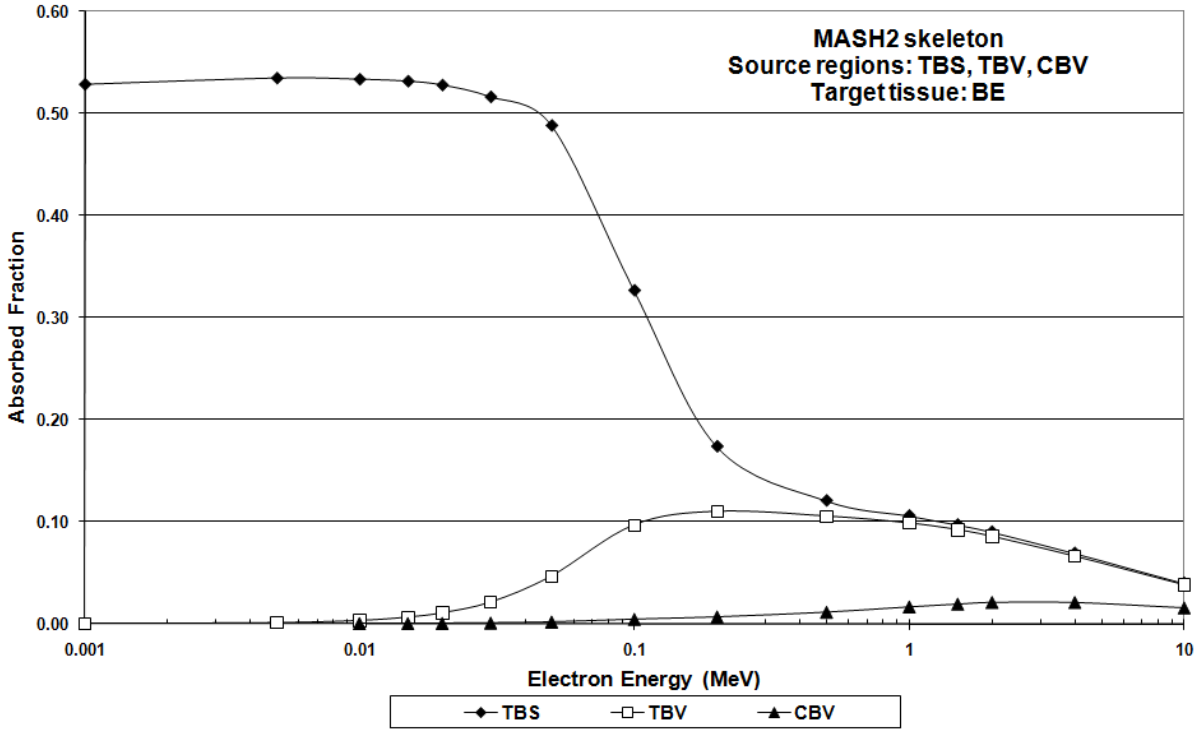

Figure 8b. Absorbed fractions of energy in the bone endosteum (BE) for electrons isotropically emitted on the trabecular bone surface (TBS), in the trabecular bone volume (TBV) and in the cortical bone volume (CBV) as a function of the electron source energy.

According to table 1, the medullary bone endosteum (MBE) mass represents only 1.5% of the total BE mass and is located at the periphery of the skeleton. It was shown earlier that for external exposure to photons between 10 keV and 10 MeV the absorbed dose to the MBE has a negligible effect on the total BE absorbed dose. For all energies, the differences between BE absorbed doses with and without the MBE were smaller than the combined statistical errors for the two cases (Kramer et al 2009a). For the internal exposure scenarios considered in this study, no differences within the combined statistical errors were found between inclusion and exclusion of the MBE for the AFs(BE←T) with T = AM, IM, TM, TBE, TBS and TBV. However, table 5 shows that significant AFs for the MBE can be seen when the CBV or the medullary CBS are the source regions. When the CBV is the source region and the electron energy is 10 keV, the MBE receives almost 15% of all the energy absorbed in the BE, because the 50 μm BE layer is located just next to the cortical bone surface. With increasing source energy, the MBE absorbed fraction decreases to 1.5% at 10 MeV, because increasingly, electrons reach more of the TBE in deeper regions of spongiosa. Medullary

CBS as source region means all or most of the emitted energy goes to the MBE. Only for energies greater than 500 keV does the TBE begin to 'see' some of these electrons, but even for 10 MeV the TBE fraction is only 38.4% according to table 5.

Table 3. Absorbed fractions of energy in the active marrow (AM) from electrons emitted in source regions TM, AM, TIM, TBE, TBS, TBV and CBV as a function of the electron energy.

E (MeV)	AF(AM←TM)	AF(AM←AM)	AF(AM←TIM)	AF(AM←TBE)	AF(AM←TBS)	AF(AM←TBV)	AF(AM←CBV)
0.001	3.85E-01	9.99E-01	4.94E-02	3.66E-01	1.93E-01	7.76E-05	
0.005	3.84E-01	9.97E-01	5.05E-02	3.65E-01	1.95E-01	4.07E-04	
0.01	3.84E-01	9.90E-01	5.37E-02	3.62E-01	1.95E-01	1.31E-03	
0.015	3.84E-01	9.78E-01	5.90E-02	3.58E-01	1.96E-01	2.76E-03	6.98E-05
0.02	3.83E-01	9.63E-01	6.55E-02	3.53E-01	1.97E-01	4.67E-03	1.38E-04
0.03	3.82E-01	9.26E-01	8.20E-02	3.41E-01	1.97E-01	9.26E-03	2.41E-04
0.05	3.79E-01	8.33E-01	1.23E-01	3.08E-01	1.98E-01	2.16E-02	5.92E-04
0.1	3.66E-01	6.45E-01	1.99E-01	2.47E-01	1.97E-01	5.81E-02	1.94E-03
0.2	3.36E-01	5.47E-01	2.07E-01	2.28E-01	2.10E-01	1.31E-01	5.60E-03
0.5	2.93E-01	4.67E-01	1.85E-01	2.30E-01	2.25E-01	2.06E-01	1.81E-02
1	2.68E-01	4.25E-01	1.71E-01	2.14E-01	2.12E-01	2.01E-01	3.29E-02
1.5	2.48E-01	3.92E-01	1.59E-01	1.98E-01	1.97E-01	1.89E-01	4.09E-02
2	2.30E-01	3.64E-01	1.48E-01	1.84E-01	1.83E-01	1.77E-01	4.45E-02
4	1.79E-01	2.84E-01	1.16E-01	1.41E-01	1.41E-01	1.38E-01	4.33E-02
10	1.11E-01	1.77E-01	7.10E-02	8.59E-02	8.59E-02	8.48E-02	3.31E-02

Table 4. Absorbed fractions of energy in the bone endosteum (BE) from electrons emitted in source regions TM, AM, TIM, TBE, TBS, TBV, CBV and CBS as a function of the electron energy.

E (MeV)	AF(BE←TM)	AF(BE←AM)	AF(BE←TIM)	AF(BE←TBE)	AF(BE←TBS)	AF(BE←TBV)	AF(BE←CBV)	AF(BE←CBS)
0.001	1.47E-01	1.41E-01	1.53E-01	9.99E-01	5.29E-01	1.79E-04		4.74E-02
0.005	1.47E-01	1.41E-01	1.52E-01	9.94E-01	5.35E-01	9.56E-04		4.73E-02
0.01	1.46E-01	1.40E-01	1.52E-01	9.80E-01	5.34E-01	2.99E-03	8.97E-05	4.72E-02
0.015	1.45E-01	1.39E-01	1.51E-01	9.57E-01	5.32E-01	6.30E-03	1.83E-04	4.72E-02
0.02	1.43E-01	1.38E-01	1.49E-01	9.30E-01	5.28E-01	1.05E-02	3.34E-04	4.70E-02
0.03	1.40E-01	1.33E-01	1.45E-01	8.60E-01	5.17E-01	2.09E-02	6.48E-04	4.64E-02
0.05	1.30E-01	1.23E-01	1.36E-01	6.91E-01	4.89E-01	4.65E-02	1.59E-03	4.49E-02
0.1	1.10E-01	1.01E-01	1.17E-01	3.63E-01	3.27E-01	9.67E-02	4.16E-03	4.05E-02
0.2	1.02E-01	9.17E-02	1.10E-01	1.86E-01	1.74E-01	1.10E-01	6.47E-03	3.62E-02
0.5	9.77E-02	8.64E-02	1.05E-01	1.24E-01	1.21E-01	1.05E-01	1.11E-02	2.68E-02
1	9.14E-02	7.97E-02	9.90E-02	1.07E-01	1.06E-01	9.84E-02	1.62E-02	1.72E-02
1.5	8.55E-02	7.37E-02	9.33E-02	9.80E-02	9.72E-02	9.20E-02	1.89E-02	1.32E-02
2	8.00E-02	6.81E-02	8.80E-02	9.08E-02	9.02E-02	8.55E-02	2.05E-02	1.11E-02
4	6.27E-02	5.22E-02	7.00E-02	6.97E-02	6.94E-02	6.60E-02	2.05E-02	7.66E-03
10	3.69E-02	3.18E-02	4.08E-02	1.25E-02	3.99E-02	3.80E-02	1.53E-02	4.92E-03

Table 5. Absorbed fractions of energy in the bone endosteum (BE) and in the trabecular bone endosteum (TBE) for electrons isotropically emitted in the cortical bone volume (CBV) and on medullary cortical bone surfaces (CBS).

E (MeV)	AF(BE←CBV)	AF(TBE←CBV)	Ratio	AF(BE←CBS)	AF(TBE←CBS)	Ratio
0.001				4.74E-02		
0.005				4.73E-02		
0.01	8.97E-05	7.64E-05	0.852	4.72E-02		
0.015	1.83E-04	1.59E-04	0.867	4.72E-02		
0.02	3.34E-04	2.97E-04	0.887	4.70E-02		
0.03	6.48E-04	5.66E-04	0.873	4.64E-02		
0.05	1.59E-03	1.38E-03	0.869	4.49E-02		
0.1	4.16E-03	3.63E-03	0.874	4.05E-02		
0.2	6.47E-03	5.76E-03	0.891	3.62E-02		
0.5	1.11E-02	1.03E-02	0.929	2.68E-02	2.09E-04	0.008
1	1.62E-02	1.54E-02	0.949	1.72E-02	3.99E-04	0.023
1.5	1.89E-02	1.82E-02	0.962	1.32E-02	5.95E-04	0.045
2	2.05E-02	1.98E-02	0.964	1.11E-02	7.76E-04	0.070
4	2.05E-02	2.00E-02	0.975	7.66E-03	1.37E-03	0.179
10	1.53E-02	1.51E-02	0.985	4.92E-03	1.89E-03	0.384

3.1.2 Secondary target tissues

AM and BE are usually of primary concern with respect to radiological protection because of the range of electrons emitted by most bone-seeking radionuclides. However, it is also important to know how the energy is absorbed beyond the limits of the skeleton. Table 6 shows absorbed fractions of energy for skeletal tissues and for organs and tissues located outside the skeleton when the trabecular marrow (TM) is the source region. Up to 50 keV, emitted energy is basically absorbed by the marrow, with a distribution between AM and TIM depending on the CFs. Here, the absorbed fractions are about 60% and 38% for the TIM and the AM, respectively, while about 2% go to the TBV. With increasing source energy, more energy is deposited first in the TBV, then in the CBV and finally to a small extent also in the cartilage and the teeth. Significant energy loss to TBV begins at around 100 keV and to CBV at around 500 keV. Up to 500 keV, essentially all energy emitted in TM is absorbed in the skeleton. 1.5% of the emitted energy escapes from the skeleton at 1 MeV, causing statistically significant AFs first of all in tissue close to the cortical bone shell, like skeletal muscle and general soft-tissue, but also in the medullary MIM. With further increase of the electron source energy, the fraction of energy leaving the skeleton rises, more organs and tissues located outside the skeleton receive AFs and finally, at 10 MeV, about 49% of the emitted energy leaves the skeleton and is distributed within muscle (21%), soft-tissue (10%), adipose (6.4%), lungs (1.8%), and others (3%), while 6.8% of the energy leaves the human body. The bone endosteum does not appear in table 6 because, being a sub-volume of the marrow, its AF is already accounted for in the AFs for AM, TIM and MIM. The BE AF has been added to figure 9, which is a graphical representation of table 6 and it can also be found in table 4. The AFs of all soft tissues in the trabecular cavities decrease slowly with increasing energy while the AFs first in bone and then also in tissues located outside the skeleton increase quickly with increasing energy. For high energies many of these AFs show values around 10%.

Table 6. MASH2: Absorbed fractions of energy from source region TM for target tissues: AM, TIM, TBV, CBV, cartilage/teeth, skeleton, brain, lungs, muscle, soft tissue, skin, adipose tissue, medullary inactive marrow, the sum of the targets, whole body and the fraction of energy which leaves the body.

Source:						TM										
Target:	AM	TIM	TBV	CBV	CAR_TEE	SKEL	BRAIN	LUNGS	MUSCLE	SOFT TISS	SKIN	ADIPOSE	MIM	SUM	WB	OUT
E (MeV)	AF	AF	AF	AF	AF	AF	AF	AF	AF	AF	AF	AF	AF	AF	AF	AF
0.001	3.85E-01	6.15E-01				1.000								1.000	1.000	0.000
0.005	3.84E-01	6.15E-01	4.15E-04	3.02E-05		1.000								1.000	1.000	0.000
0.01	3.84E-01	6.14E-01	1.14E-03	8.75E-05		1.000								1.000	1.000	0.000
0.015	3.84E-01	6.13E-01	2.49E-03	1.96E-04	1.22E-05	1.000								1.000	1.000	0.000
0.02	3.83E-01	6.12E-01	4.13E-03	3.35E-04	1.97E-05	1.000								1.000	1.000	0.000
0.03	3.82E-01	6.09E-01	8.47E-03	6.85E-04	4.68E-05	1.000								1.000	1.000	0.000
0.05	3.79E-01	6.00E-01	1.96E-02	1.70E-03	9.50E-05	1.000								1.000	1.000	0.000
0.1	3.66E-01	5.74E-01	5.48E-02	5.39E-03	3.54E-04	1.000								1.000	1.000	0.000
0.2	3.36E-01	5.19E-01	1.27E-01	1.58E-02	1.06E-03	0.999			1.55E-04	1.62E-04		2.71E-05	1.67E-04	1.000	1.000	0.000
0.5	2.93E-01	4.51E-01	1.99E-01	5.02E-02	3.56E-03	0.996		1.84E-05	1.13E-03	9.22E-04	1.11E-05	1.31E-04	4.98E-04	0.999	0.999	0.001
1.0	2.68E-01	4.19E-01	1.96E-01	9.46E-02	7.82E-03	0.985	2.37E-05	7.71E-05	6.78E-03	4.71E-03	3.58E-05	6.35E-04	1.11E-03	0.998	0.998	0.002
1.5	2.48E-01	3.93E-01	1.85E-01	1.22E-01	1.18E-02	0.959	1.34E-04	3.30E-04	1.98E-02	1.34E-02	1.09E-04	2.10E-03	1.63E-03	0.997	0.997	0.003
2.0	2.30E-01	3.69E-01	1.74E-01	1.37E-01	1.54E-02	0.925	4.71E-04	9.78E-04	3.70E-02	2.39E-02	3.03E-04	4.56E-03	2.14E-03	0.995	0.996	0.004
4.0	1.79E-01	2.92E-01	1.38E-01	1.45E-01	2.72E-02	0.782	2.80E-03	6.33E-03	1.07E-01	6.11E-02	2.13E-03	2.05E-02	3.30E-03	0.984	0.987	0.013
10.0	1.11E-01	1.69E-01	8.18E-02	1.14E-01	3.22E-02	0.508	6.56E-03	1.84E-02	2.10E-01	9.89E-02	8.76E-03	6.43E-02	3.48E-03	0.918	0.932	0.068

Table 7. MASH2: Absorbed fractions of energy from source region AM for target tissues: AM, TIM, TBV, CBV, cartilage/teeth, skeleton, brain, lungs, muscle, soft tissue, skin, adipose tissue, medullary inactive marrow, the sum of the targets, whole body and the fraction of energy which leaves the body.

Source						AM										
Target:	AM	TIM	TBV	CBV	CAR_TEE	SKEL	BRAIN	LUNGS	MUSCLE	SOFT TISS	SKIN	ADIPOSE	MIM	SUM	WB	OUT
E (MeV)	AF	AF	AF	AF	AF	AF	AF	AF	AF	AF	AF	AF	AF	AF	AF	AF
0.001	9.99E-01	5.45E-04	6.42E-05			1.000								1.000	1.000	0.000
0.005	9.97E-01	2.84E-03	3.34E-04	3.14E-05		1.000								1.000	1.000	0.000
0.01	9.90E-01	9.07E-03	1.10E-03	1.02E-04		1.000								1.000	1.000	0.000
0.015	9.78E-01	1.97E-02	2.35E-03	2.21E-04	2.09E-05	1.000								1.000	1.000	0.000
0.02	9.63E-01	3.29E-02	3.97E-03	3.66E-04	3.38E-05	1.000								1.000	1.000	0.000
0.03	9.26E-01	6.54E-02	8.04E-03	7.63E-04	7.40E-05	1.000								1.000	1.000	0.000
0.05	8.33E-01	1.46E-01	1.87E-02	1.87E-03	1.90E-04	1.000								1.000	1.000	0.000
0.1	6.45E-01	2.98E-01	5.04E-02	6.06E-03	5.91E-04	1.000								1.000	1.000	0.000
0.2	5.47E-01	3.18E-01	1.15E-01	1.75E-02	1.84E-03	0.999			2.02E-04	2.75E-04		3.55E-05		1.000	1.000	0.000
0.5	4.67E-01	2.86E-01	1.81E-01	5.59E-02	6.42E-03	0.996		2.56E-05	1.59E-03	1.38E-03	1.20E-05	1.18E-04	1.04E-04	0.999	0.999	0.001
1.0	4.25E-01	2.64E-01	1.77E-01	1.02E-01	1.33E-02	0.981	2.20E-05	1.10E-04	9.13E-03	6.93E-03	1.89E-05	5.73E-04	2.20E-04	0.998	0.998	0.002
1.5	3.92E-01	2.44E-01	1.66E-01	1.27E-01	1.92E-02	0.949	1.33E-04	5.53E-04	2.62E-02	1.90E-02	4.63E-05	1.91E-03	3.65E-04	0.997	0.997	0.003
2.0	3.64E-01	2.27E-01	1.55E-01	1.38E-01	2.32E-02	0.907	4.54E-04	1.56E-03	4.79E-02	3.33E-02	9.80E-05	4.38E-03	4.46E-04	0.995	0.996	0.004
4.0	2.84E-01	1.76E-01	1.21E-01	1.35E-01	3.06E-02	0.746	2.80E-03	1.02E-02	1.25E-01	7.87E-02	9.64E-04	2.05E-02	7.47E-04	0.985	0.989	0.011
10.0	1.77E-01	1.08E-01	7.48E-02	1.03E-01	2.72E-02	0.490	6.68E-03	3.12E-03	2.18E-01	1.19E-01	4.05E-03	6.38E-02	8.22E-04	0.905	0.953	0.047

Table 8. MASH2: Absorbed fractions of energy from source region CBV for target tissues: AM, TIM, TBV, CBV, cartilage/teeth, skeleton, brain, lungs, muscle, soft tissue, skin, adipose tissue, medullary inactive marrow, the sum of the targets, whole body and the fraction of energy which leaves the body.

Source:						CBV									
Target:	AM	TIM	TBV	CBV	CAR_TEE	SKEL	BRAIN	LUNGS	MUSCLE	SOFT TISS	SKIN	ADIPOSE	MIM	SUM	WB	OUT
E (MeV)	AF	AF	AF	AF	AF	AF	AF	AF	AF	AF	AF	AF	AF	AF	AF	AF
0.001				1.00E+00		1.000								1.000	1.000	0.000
0.005				1.00E+00		1.000								1.000	1.000	0.000
0.01				1.00E+00		1.000								1.000	1.000	0.000
0.015	6.98E-05	8.95E-05	3.91E-05	9.99E-01	2.29E-05	1.000								1.000	1.000	0.000
0.02	1.38E-04	1.60E-04	6.11E-05	9.99E-01	3.78E-05	0.999								0.999	1.000	0.000
0.03	2.41E-04	3.30E-04	1.29E-04	9.98E-01	9.30E-05	0.999			5.61E-04	3.22E-04		1.39E-04		1.000	1.000	0.000
0.05	5.92E-04	7.94E-04	3.45E-04	9.95E-01	2.05E-04	0.997			1.37E-03	7.73E-04		3.19E-04		1.000	1.000	0.000
0.1	1.94E-03	2.49E-03	1.09E-03	9.85E-01	6.42E-04	0.991			4.34E-03	2.44E-03	3.15E-05	1.05E-03	1.82E-04	0.999	0.999	0.001
0.2	5.60E-03	7.28E-03	3.62E-03	9.55E-01	2.02E-03	0.973	2.02E-05		1.32E-02	7.46E-03	9.99E-05	3.08E-03	1.45E-03	0.999	0.999	0.001
0.5	1.81E-02	2.33E-02	1.42E-02	8.48E-01	6.84E-03	0.910	4.76E-05	9.95E-05	4.39E-02	2.49E-02	3.17E-04	1.08E-02	6.68E-03	0.997	0.998	0.002
1.0	3.29E-02	4.47E-02	2.89E-02	6.98E-01	1.40E-02	0.818	1.23E-03	4.47E-04	8.83E-02	4.80E-02	1.03E-03	2.24E-02	1.48E-02	0.994	0.996	0.004
1.5	4.09E-02	5.87E-02	3.83E-02	5.88E-01	2.01E-02	0.746	4.32E-03	1.13E-03	1.23E-01	6.08E-02	2.56E-03	3.28E-02	2.09E-02	0.991	0.994	0.006
2.0	4.45E-02	6.78E-02	4.42E-02	5.07E-01	2.41E-02	0.687	7.84E-03	1.96E-03	1.50E-01	6.84E-02	4.83E-03	4.15E-02	2.50E-02	0.987	0.991	0.009
4.0	4.33E-02	7.54E-02	4.77E-02	3.42E-01	2.93E-02	0.538	2.03E-02	6.18E-03	2.14E-01	7.98E-02	1.16E-02	6.16E-02	2.84E-02	0.959	0.968	0.032
10.0	3.31E-02	6.00E-02	3.71E-02	1.97E-01	2.58E-02	0.353	3.51E-02	3.51E-02	2.53E-01	8.01E-02	1.76E-02	8.50E-02	1.83E-02	0.877	0.870	0.130

Table 9. MASH2: Absorbed fractions of energy from source region TBE for target tissues: AM, TIM, TBV, CBV, cartilage/teeth, skeleton, brain, lungs, muscle, soft tissue, skin, adipose tissue, medullary inactive marrow, the sum of the targets, whole body and the fraction of energy which leaves the body.

Source:						TBE									
Target:	AM	TIM	TBV	CBV	CAR_TEE	SKEL	BRAIN	LUNGS	MUSCLE	SOFT TISS	SKIN	ADIPOSE	MIM	SUM	WB	OUT
E (MeV)	AF	AF	AF	AF	AF	AF	AF	AF	AF	AF	AF	AF	AF	AF	AF	AF
0.001	3.66E-01	6.34E-01				1.000								1.000	1.000	0.000
0.005	3.65E-01	6.33E-01	2.74E-03			1.000								1.000	1.000	0.000
0.01	3.62E-01	6.29E-01	8.78E-03			1.000								1.000	1.000	0.000
0.015	3.58E-01	6.23E-01	1.88E-02			1.000								1.000	1.000	0.000
0.02	3.53E-01	6.16E-01	3.11E-02			1.000								1.000	1.000	0.000
0.03	3.41E-01	5.97E-01	6.24E-02			1.000								1.000	1.000	0.000
0.05	3.08E-01	5.52E-01	1.41E-01			1.000								1.000	1.000	0.000
0.1	2.47E-01	4.60E-01	2.93E-01	6.02E-04		1.000								1.000	1.000	0.000
0.2	2.28E-01	4.41E-01	3.22E-01	8.63E-03	3.10E-04	0.999			1.06E-04	6.80E-05				1.000	1.000	0.000
0.5	2.30E-01	4.48E-01	2.69E-01	4.79E-02	1.84E-03	0.997	1.46E-05		9.16E-04	6.08E-04	1.16E-05	1.41E-04	4.89E-04	0.999	0.999	0.001
1.0	2.14E-01	4.25E-01	2.46E-01	9.70E-02	4.70E-03	0.986	4.07E-05	5.72E-05	6.10E-03	3.64E-03	3.47E-05	7.35E-04	1.22E-03	0.998	0.998	0.002
1.5	1.98E-01	4.01E-01	2.28E-01	1.28E-01	7.68E-03	0.962	2.69E-04	2.81E-04	1.91E-02	1.07E-02	1.26E-04	2.58E-03	1.77E-03	0.996	0.997	0.003
2.0	1.84E-01	3.77E-01	2.11E-01	1.46E-01	1.06E-02	0.929	9.24E-04	8.17E-04	3.63E-02	1.96E-02	3.62E-04	5.58E-03	2.31E-03	0.995	0.995	0.005
4.0	1.41E-01	2.99E-01	1.63E-01	1.57E-01	2.24E-02	0.783	5.60E-03	5.52E-03	1.09E-01	5.13E-02	2.66E-03	2.24E-02	3.54E-03	0.983	0.986	0.014
10.0	8.59E-02	1.73E-01	9.37E-02	1.22E-01	2.96E-02	0.504	1.31E-02	1.48E-02	2.15E-01	8.66E-02	9.82E-03	6.40E-02	3.83E-03	0.911	0.924	0.076

Table 10. MASH2: Absorbed fractions of energy from source region TBS for target tissues: AM, TIM, TBV, CBV, cartilage/teeth, skeleton, brain, lungs, muscle, soft tissue, skin, adipose tissue, medullary inactive marrow, the sum of the targets, whole body and the fraction of energy which leaves the body.

Source:						TBS										
Target:	AM	TIM	TBV	CBV	CAR_TEE	SKEL	BRAIN	LUNGS	MUSCLE	SOFT TISS	SKIN	ADIPOSE	MIM	SUM	WB	OUT
E (MeV)	AF	AF	AF	AF	AF	AF	AF	AF	AF	AF	AF	AF	AF	AF	AF	AF
0.001	1.93E-01	3.37E-01	4.71E-01			1.000								1.000	1.000	0.000
0.005	1.95E-01	3.41E-01	4.64E-01			1.000								1.000	1.000	0.000
0.01	1.95E-01	3.43E-01	4.62E-01			1.000								1.000	1.000	0.000
0.015	1.96E-01	3.45E-01	4.59E-01			1.000								1.000	1.000	0.000
0.02	1.97E-01	3.46E-01	4.57E-01			1.000								1.000	1.000	0.000
0.03	1.97E-01	3.49E-01	4.54E-01	2.20E-05		1.000								1.000	1.000	0.000
0.05	1.98E-01	3.56E-01	4.46E-01	5.97E-05		1.000								1.000	1.000	0.000
0.1	1.97E-01	3.69E-01	4.33E-01	4.66E-04	1.78E-05	1.000								1.000	1.000	0.000
0.2	2.10E-01	4.08E-01	3.73E-01	8.03E-03	2.91E-04	0.999			1.10E-04	7.20E-05		3.05E-05	8.07E-05	1.000	1.000	0.000
0.5	2.25E-01	4.41E-01	2.82E-01	4.72E-02	1.89E-03	0.997	1.56E-05	1.77E-05	9.23E-04	5.86E-04	1.27E-05	1.37E-04	5.12E-04	0.999	0.999	0.001
1.0	2.12E-01	4.22E-01	2.52E-01	9.58E-02	4.65E-03	0.986	3.78E-05	5.31E-05	6.08E-03	3.63E-03	3.50E-05	7.58E-04	1.20E-03	0.998	0.998	0.002
1.5	1.97E-01	3.98E-01	2.32E-01	1.28E-01	7.56E-03	0.962	2.68E-04	2.78E-04	1.87E-02	1.06E-02	1.24E-04	2.59E-03	1.79E-03	0.996	0.997	0.003
2.0	1.83E-01	3.76E-01	2.15E-01	1.46E-01	1.06E-02	0.929	8.92E-04	8.57E-04	3.60E-02	1.96E-02	3.47E-04	5.50E-03	2.29E-03	0.995	0.995	0.005
4.0	1.41E-01	2.98E-01	1.65E-01	1.57E-01	2.24E-02	0.783	5.63E-03	5.49E-03	1.08E-01	5.11E-02	2.64E-03	2.24E-02	3.59E-03	0.982	0.986	0.014
10.0	8.59E-02	1.73E-01	9.43E-02	1.22E-01	2.97E-02	0.505	1.31E-02	1.50E-02	2.15E-01	8.63E-02	9.82E-03	6.40E-02	3.82E-03	0.911	0.924	0.076

Table 11. MASH2: Absorbed fractions of energy from source region TBV for target tissues: AM, TIM, TBV, CBV, cartilage/teeth, skeleton, brain, lungs, muscle, soft tissue, skin, adipose tissue, medullary inactive marrow, the sum of the targets, whole body and the fraction of energy which leaves the body.

Source:						TBV									
Target:	AM	TIM	TBV	CBV	CAR_TEE	SKEL	BRAIN	LUNGS	MUSCLE	SOFT TISS	SKIN	ADIPOSE	MIM	SUM	WB	OUT
E (MeV)	AF	AF	AF	AF	AF	AF	AF	AF	AF	AF	AF	AF	AF	AF	AF	AF
0.001			1.00E+00			1.000								1.000	1.000	0.000
0.005	4.07E-04	7.14E-04	9.99E-01	1.92E-05		1.000								1.000	1.000	0.000
0.01	1.31E-03	2.16E-03	9.97E-01	5.86E-05		1.000								1.000	1.000	0.000
0.015	2.76E-03	4.64E-03	9.93E-01	1.33E-04		1.000								1.000	1.000	0.000
0.02	4.67E-03	7.73E-03	9.87E-01	2.27E-04		1.000								1.000	1.000	0.000
0.03	9.26E-03	1.57E-02	9.75E-01	4.52E-04	1.71E-05	1.000								1.000	1.000	0.000
0.05	2.16E-02	3.64E-02	9.41E-01	1.14E-03	3.56E-05	1.000								1.000	1.000	0.000
0.1	5.81E-02	1.03E-01	8.35E-01	3.87E-03	1.34E-04	1.000								1.000	1.000	0.000
0.2	1.31E-01	2.39E-01	6.16E-01	1.27E-02	3.96E-04	0.999	1.43E-05		1.29E-04	9.50E-05		4.48E-05	8.33E-05	1.000	1.000	0.000
0.5	2.06E-01	3.70E-01	3.70E-01	4.98E-02	1.89E-03	0.997	3.41E-05	1.15E-05	7.70E-04	6.93E-04	1.35E-05	1.84E-04	4.13E-04	0.999	0.999	0.001
1.0	2.01E-01	3.65E-01	3.15E-01	1.02E-01	4.69E-03	0.987	1.00E-04	4.50E-05	4.62E-03	4.02E-03	3.61E-05	1.12E-03	9.26E-04	0.998	0.998	0.002
1.5	1.89E-01	3.47E-01	2.84E-01	1.36E-01	7.29E-03	0.964	6.39E-04	2.09E-04	1.42E-02	1.19E-02	1.23E-04	3.96E-03	1.43E-03	0.996	0.997	0.003
2.0	1.77E-01	3.28E-01	2.60E-01	1.56E-01	1.02E-02	0.931	2.24E-03	6.15E-04	2.81E-02	2.16E-02	3.86E-04	8.77E-03	1.82E-03	0.994	0.995	0.005
4.0	1.38E-01	2.61E-01	1.93E-01	1.68E-01	2.06E-02	0.781	1.41E-02	3.90E-03	8.84E-02	5.35E-02	3.61E-03	3.11E-02	2.87E-03	0.979	0.983	0.017
10.0	8.48E-02	1.51E-01	1.08E-01	1.31E-01	2.65E-02	0.502	3.34E-02	1.14E-02	1.81E-01	8.47E-02	1.04E-02	7.11E-02	3.05E-03	0.897	0.913	0.087

Table 12. MASH2: Absorbed fractions of energy from source region TIM for target tissues: AM, TIM, TBV, CBV, cartilage/teeth, skeleton, brain, lungs, muscle, soft tissue, skin, adipose tissue, medullary inactive marrow, the sum of the targets, whole body and the fraction of energy which leaves the body.

Source:						TIM										
Target:	AM	TIM	TBV	CBV	CAR_TEE	SKEL	BRAIN	LUNGS	MUSCLE	SOFT TISS	SKIN	ADIPOSE	MIM	SUM	WB	OUT
E (MeV)	AF	AF	AF	AF	AF	AF	AF	AF	AF	AF	AF	AF	AF	AF	AF	AF
0.001	4.94E-02	9.51E-01				1.000								1.000	1.000	0.000
0.005	5.05E-02	9.49E-01	3.90E-04	2.71E-05		1.000								1.000	1.000	0.000
0.01	5.37E-02	9.45E-01	1.18E-03	8.84E-05		1.000								1.000	1.000	0.000
0.015	5.90E-02	9.38E-01	2.60E-03	1.75E-04		1.000								1.000	1.000	0.000
0.02	6.55E-02	9.30E-01	4.33E-03	3.14E-04		1.000								1.000	1.000	0.000
0.03	8.20E-02	9.09E-01	8.79E-03	6.42E-04		1.000								1.000	1.000	0.000
0.05	1.23E-01	8.55E-01	2.07E-02	1.58E-03	5.10E-05	1.000								1.000	1.000	0.000
0.1	1.99E-01	7.38E-01	5.78E-02	4.94E-03	1.66E-04	1.000								1.000	1.000	0.000
0.2	2.07E-01	6.43E-01	1.34E-01	1.44E-02	5.00E-04	0.999			1.34E-04	1.08E-04		2.83E-05	2.36E-04	1.000	1.000	0.000
0.5	1.85E-01	5.55E-01	2.09E-01	4.61E-02	1.70E-03	0.997			8.58E-04	6.12E-04	1.25E-05	1.32E-04	7.80E-04	0.999	0.999	0.001
1.0	1.71E-01	5.16E-01	2.07E-01	8.83E-02	4.05E-03	0.987	2.17E-05	4.90E-05	5.18E-03	3.34E-03	4.94E-05	6.20E-04	1.75E-03	0.998	0.998	0.002
1.5	1.59E-01	4.87E-01	1.97E-01	1.16E-01	7.09E-03	0.966	1.33E-04	1.89E-04	1.55E-02	9.70E-03	1.65E-04	2.19E-03	2.54E-03	0.996	0.997	0.003
2.0	1.48E-01	4.60E-01	1.87E-01	1.33E-01	1.02E-02	0.938	4.52E-04	6.01E-04	2.98E-02	1.79E-02	4.06E-04	4.63E-03	3.28E-03	0.995	0.995	0.005
4.0	1.16E-01	3.67E-01	1.49E-01	1.49E-01	2.42E-02	0.805	2.71E-03	3.77E-03	9.48E-02	5.00E-02	2.70E-03	1.94E-02	5.17E-03	0.984	0.986	0.014
10.0	7.10E-02	2.11E-01	8.73E-02	1.20E-01	3.40E-02	0.523	6.21E-03	1.02E-02	2.08E-01	8.61E-02	1.12E-02	6.21E-02	5.49E-03	0.913	0.922	0.078

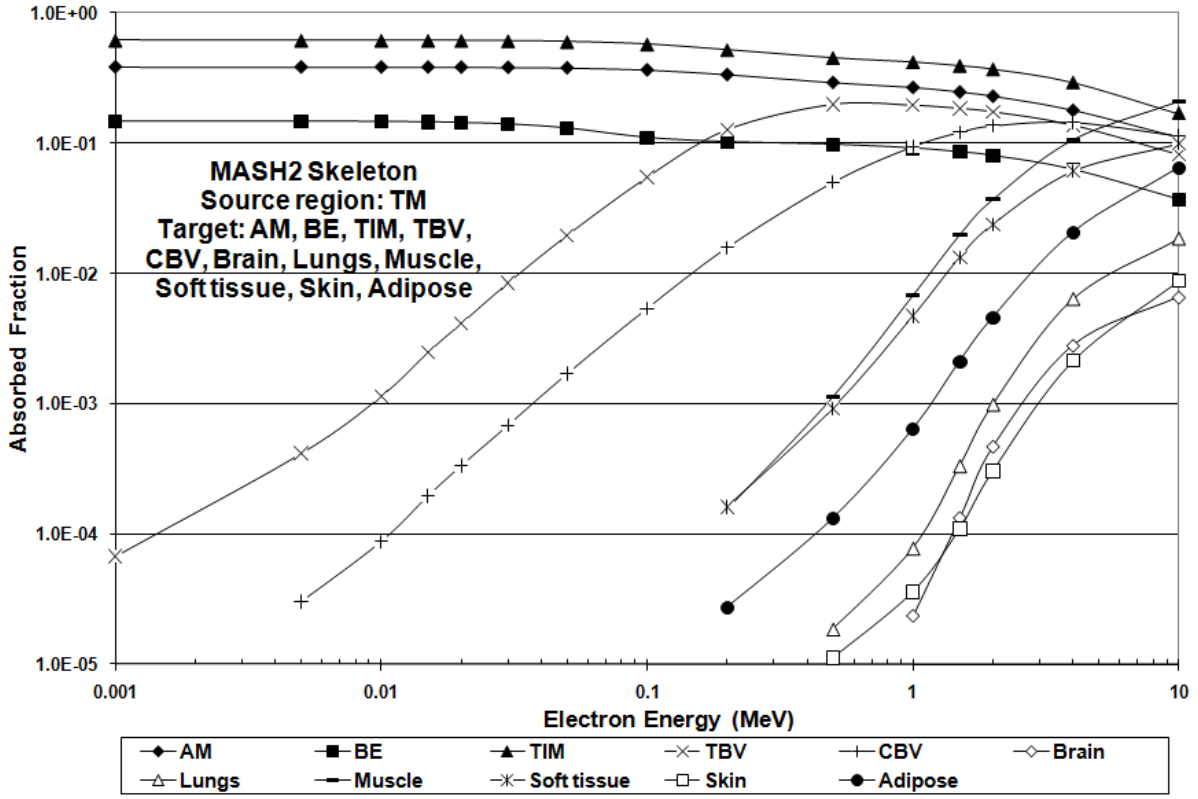

Figure 9. Absorbed fractions of energy in the active marrow (AM), the bone endosteum (BE), the trabecular inactive marrow (TIM), the trabecular bone volume (TBV), the cortical bone volume (CBV), the brain, the lungs, muscle tissue, soft tissue, skin and adipose tissue for electrons isotropically emitted in the trabecular marrow (TM)as a function of the electron source energy.

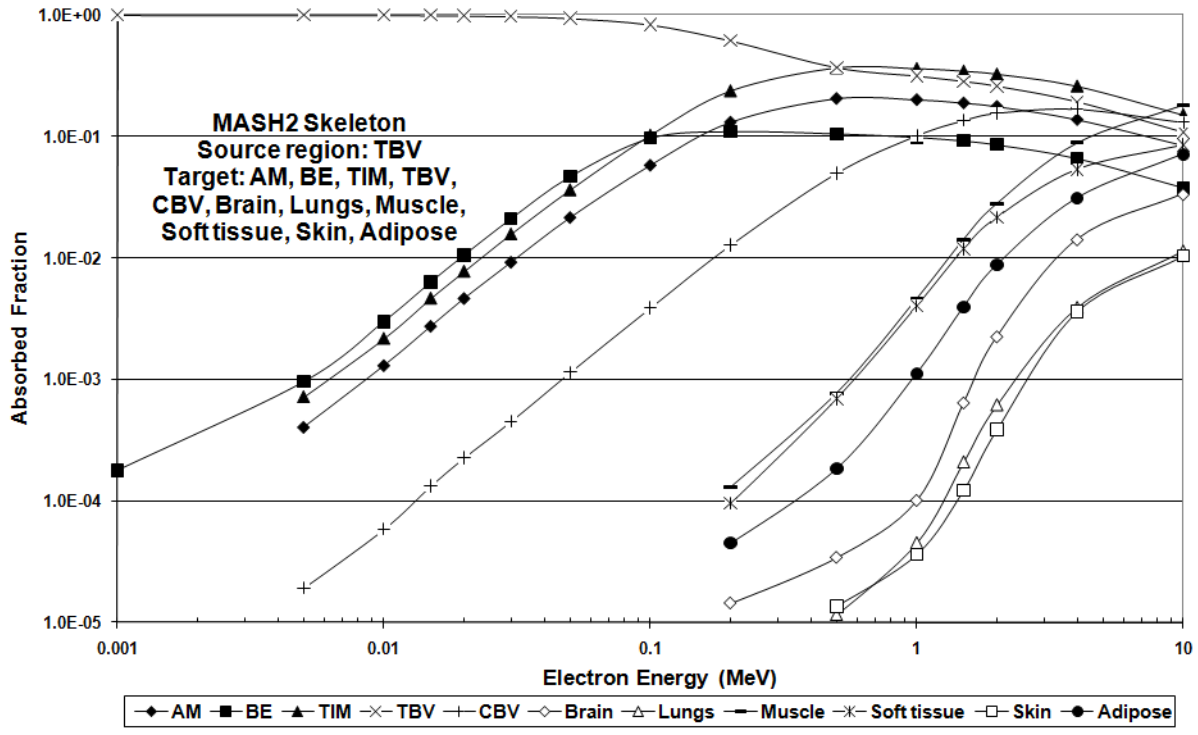

Figure 10. Absorbed fractions of energy in the active marrow (AM), the bone endosteum (BE), the trabecular inactive marrow (TIM), the trabecular bone volume (TBV), the cortical bone volume (CBV), the brain, the lungs, muscle tissue, soft tissue, skin and adipose tissue for electrons isotropically emitted in the trabecular bone volume (TBV) as a function of the electron source energy.

Figure 10 represents the case when the TBV is the source region. The AF in the TBV decreases with increasing energy. At the same time first the AFs for AM, BE and TIM increase, the AF for the CBV and finally the AFs for the tissues located outside the skeleton. The exact accounting for the deposition of energy for all source regions can be found in tables 6-12, which show that for source energy of 10 MeV the energy leaving the skeleton is about 50% for all source regions, except for the CBV where this fraction is 65%.

3.2 S-values

Absorbed doses per unit activity, also called S-values, in the AM and the BE were calculated for the electron-emitting radionuclides ^{14}C, ^{59}Fe, ^{131}I, ^{89}Sr, ^{32}P and ^{90}Y, distributed homogeneously in the source regions AM, TBS and TBV of the MASH2 skeleton. Half-lifes of the isotopes are 5730 years, 44.5, 8.0, 50.7, 14.3 and 2.7 days for ^{14}C, ^{59}Fe, ^{131}I, ^{89}Sr, ^{32}P and ^{90}Y, respectively. Although different radionuclides preferably concentrate in the bone volume (^{14}C, ^{89}Sr, ^{32}P, ^{90}Y), on the bone surface (^{90}Y) or in the marrow (^{59}Fe, ^{131}I), S-values are usually systematically calculated for several source regions because of temporal variation in radionuclide uptake. Often, the initial uptake is on the bone surface and after some time radionuclides, by bone remodelling and via bone fluid, infiltrate the bone volume and/or the marrow. Electron source energies were sampled from spectra published in ICRP Publication 107 (ICRP 2008). The gamma emission was also taken into account with mean photon energies and mean yields of 1154 keV and 0.494 Bq-s $^{-1}$, respectively, for ^{59}Fe and 380 keV and 0.712 Bq-s $^{-1}$, respectively, for ^{131}I. Table 13 shows S-values for the AM and the BE when AM, TBS and TBV are the source regions. Generally, absorbed dose per unit activity increases with increasing electron source energy. Compared to the mean cavity width of 1170 μm mentioned above, the BE thickness in the cavity is almost 12 times smaller. Nevertheless, according to table 13, the BE S-values are about 50% of the AM S-values when the AM is the source region. The explanation comes from the definition of the bone endosteum as a sub-region of the marrow, which leads to the emission of particles also in the BE region, which in turn causes significant absorbed dose to the BE. When the TBS or the TBV are the source regions, the BE S-values are always greater than the AM S-values because of the proximity of the BE to the bone surface. Electrons leaving the bone surface distribute their energy first of all across the 50 μm layer, especially for low energies. Consequently, for ^{14}C the S(BE←TBS)) is more than 6 times greater than the S(AM←TBS). With increasing energy this difference becomes smaller and for ^{90}Y the ratio of the S-values for AM and BE has decreased to 1.3. High energy electrons deposit their energy almost uniformly across the cavity. For TBV as source region one finds similar ratios between S(BE←TBV) and S(AM←TBV).

Table 13. S-values for the active marrow (AM) and the bone endosteum (BE) of the MASH2 skeleton for six radionuclides distributed homogeneously in the AM, on the trabecular bone surface (TBS) and in the trabecular bone volume (TBV).

Radionuclide	Mean Beta Energy (MeV)	MASH2 S(AM←AM) (mGy/MBq-s)	MASH2 S(BE←AM) (mGy/MBq-s)	MASH2 S(AM←TBS) (mGy/MBq-s)	MASH2 S(BE←TBS) (mGy/MBq-s)	MASH2 S(AM←TBV) (mGy/MBq-s)	MASH2 S(BE←TBV) (mGy/MBq-s)
C-14	0.050	5.18E-06	2.03E-06	1.38E-06	7.45E-06	2.75E-07	1.25E-06
Fe-59*	0.118	1.22E-05	3.22E-06	4.74E-06	1.14E-05	3.20E-06	5.65E-06
I-131*	0.192	1.42E-05	6.32E-06	5.70E-06	1.23E-05	4.08E-06	7.08E-06
Sr-89	0.585	3.64E-05	1.74E-05	1.75E-05	2.47E-05	1.60E-05	2.13E-05
P-32	0.695	4.22E-05	2.05E-05	2.06E-05	2.82E-05	1.91E-05	2.52E-05
Y-90	0.933	5.38E-05	2.61E-05	2.66E-05	3.54E-05	2.53E-05	3.24E-05

* includes also the gamma component

3.3 Comparison with other investigations

Using the trabecular microstructure information provided by the chord length distributions as a starting point, in the 80's Eckerman and co-workers from the ORNL and in the 90's Bolch and co-workers from the UF began to continue work on skeletal dosimetry pioneered by Spiers' group in Leeds. Later, Bolch's group replaced the chord length distributions with μCT images of trabecular bone. However, in the publications of both groups, one can observe differences in the modelling of the skeletal tissues, beyond the question whether to use chord length distributions or μCT images. In the studies of Spiers and co-workers it was assumed that the bone endosteum is a sub-volume of the marrow which completely fills the trabecular cavity. Eckerman and co-workers from the ORNL used the Leeds model, which today also reflects the view of the ICRP (ICRP 2009). On the other hand, Bolch's group made a distinction between cavity volume and marrow space, assuming that the endosteum is a layer of cells filling the space between the trabecular bone surface and the marrow. The two groups finally discussed these and other differences between their skeletal dosimetry models in a joint paper (Stabin et al 2002). Meanwhile the statement of ICRP110 has clarified the issue as: "A sub-region of the bone marrow, 50 μm from the bone surface, is further defined as the endosteal tissues" (ICRP 2009). However, knowledge of the differences between the Leeds and the UF model is important for the modelling of the comparative calculations performed for this study. The MC code with the 8 SP cluster method uses the ICRP110 model, but was modified to permit calculations also based on the UF model. In all comparative calculations shown here, the thickness of the BE was changed to 10 μm. It should be mentioned that comparison with data from other investigators is difficult if the data are presented only graphically. Therefore, preference was given to publications which also present the AFs in tables. Additionally, a comparison between S-values calculated with the MASH2 exposure model and with the OLINDA software (Stabin et al 2005) will be shown.

3.3.1 Comparison with ORNL data

Figures 11 and 12 show comparisons between AFs in the AM and the BE for the MASH2 and the ORNL adult skeletons (Eckerman and Stabin 2000, Stabin et al 2002) for source regions TBS, TBV and AM. Electron escape to cortical bone was not taken into account in the ORNL model and therefore all ORNL AFs in the two figures remain constant for energies higher than 500 keV. For energies up to 500 keV one finds the following average differences between the MASH2 and the ORNL AFs: 11.3%, 5.1%, 6.5% for AF(AM←TBS), AF(AM←TBV), AF(AM←AM), respectively, and 10.6%, 8.4%, 17.2% for AF(BE←TBS), AF(BE←TBV), AF(BE←AM), respectively. One has to keep in mind that the ORNL method is based on the Leeds chord length distributions using a linear one-dimensional transport model with CSDA energy-range relationships and assuming straight paths of the electrons through trabecular bone, while the 8SP cluster method applies a three-dimensional Monte Carlo method with electron straggling, scattering, back-scattering, delta rays, bremsstrahlung photons, etc. Also, some trabecular bone volume fractions (TBVFs), a influential parameter for skeletal dosimetry as the next section will show, were quite different in the two models: pelvis(ORNL) TBVF = 0.018, pelvis(MASH2) TBVF = 0.211, cranium(ORNL) TBVF = 0.026, cranium(MASH2) TBVF = 0.516, for example. In view of these methodological differences the comparisons shown in figure 11 and 12 can be considered satisfactory.

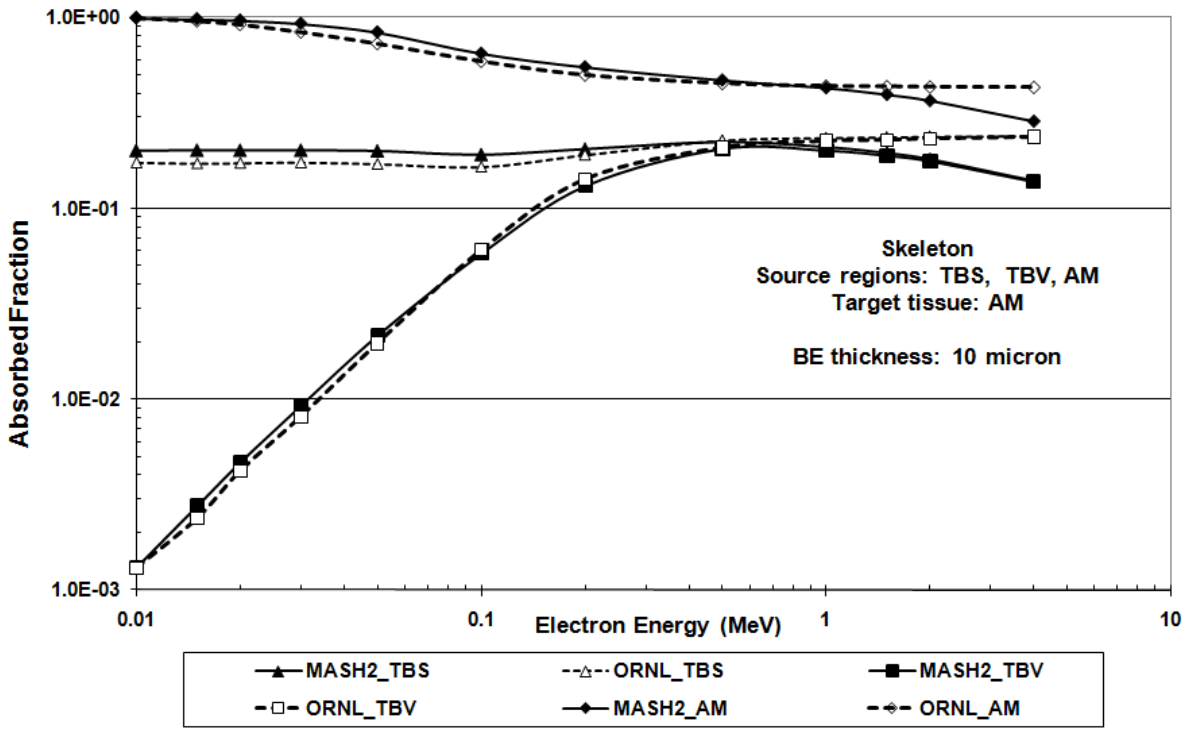

Figure 11. Absorbed fraction of energy in the active marrow (AM) of the skeleton for electrons isotropically emitted on the trabecular bone surface (TBS), in the trabecular bone volume (TBV) and in the active marrow (AM) as a function of the electron source energy. AFs are shown for the MASH2 and for the adult ORNL skeletons.

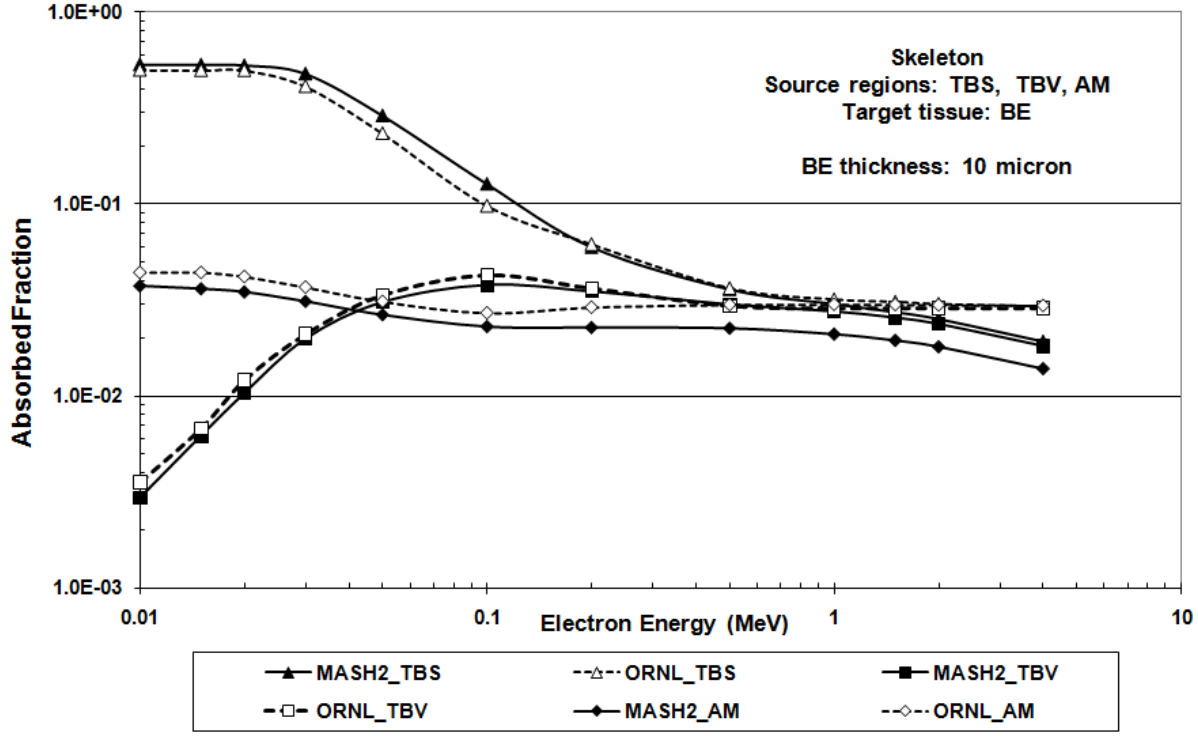

Figure 12. Absorbed fraction of energy in the bone endosteum (BE) of the skeleton for electrons isotropically emitted on the trabecular bone surface (TBS), in the trabecular bone volume (TBV) and in the active marrow (AM) as a function of the electron source energy. AFs are shown for the MASH2 and for the adult ORNL skeletons.

3.3.2 Comparison with UF data

From various UF studies using 3D μCT or μNMR images for skeletal dosimetry, the paper from Bolch et al (2002) presents tabulated AFs(AM←AM) of monoenergetic electrons emitted within the active bone marrow irradiating the active bone marrow of a femoral adult head, calculated with an "EGS4 macrostructural transport model", which takes electron escape to the cortical bone cortex into account. The bone sample was scanned at 88 μm cubic voxel resolution and the TBVF was 37%. The comparison is made for 100% cellularity, i.e. that the active marrow volume equals the marrow volume. The TBVF in the MASH2 femur was 15.2%.

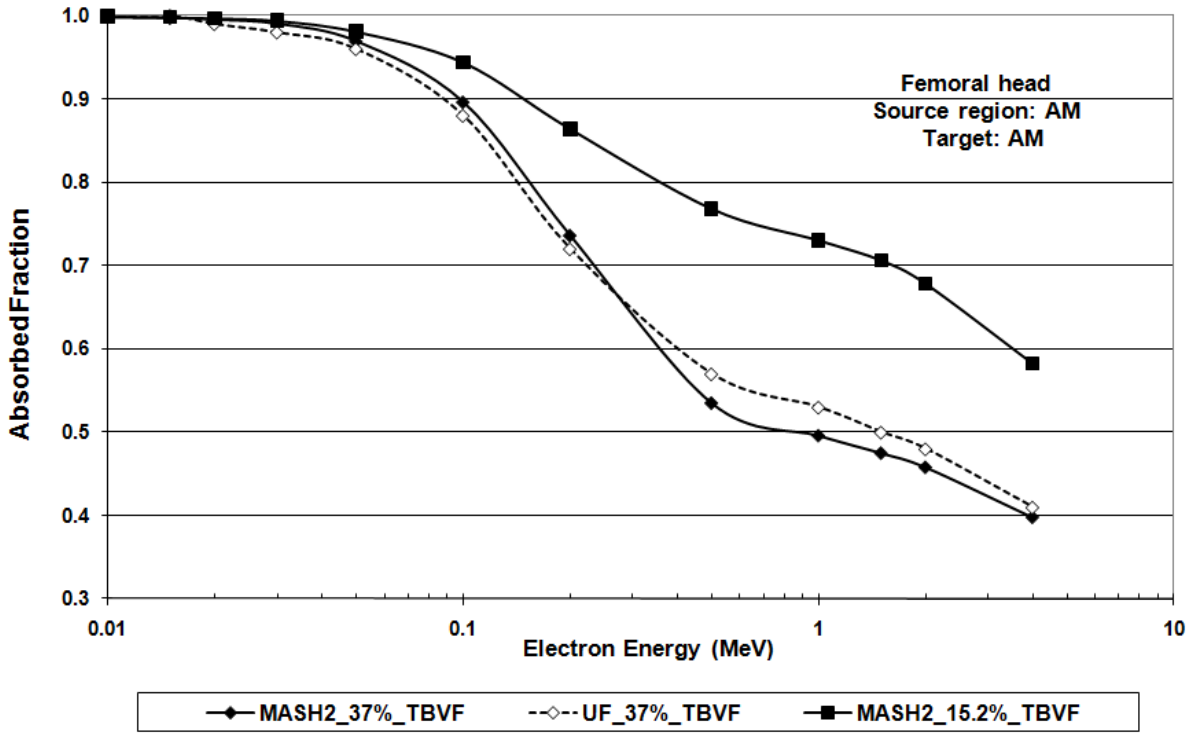

Figure 13. Absorbed fraction of energy in the active marrow (AM) of an adult femoral head for electrons isotropically emitted in the active marrow (AM) as a function of the electron source energy. AFs are shown for the MASH2 upper femur and for the UF adult femoral head. Cellularity = 100%

Figure 13 shows the AFs(AM←AM) for the spongiosa in the upper half of the MASH2 femur with 15.2% TBVF and for the UF femoral head with 37% TBVF. The disagreement is significant: 7%, 26% and 30% at 0.1, 0.5 and 4.0 MeV, respectively. Obviously having less trabecular bone in spongiosa means that more and higher energized electrons reach neighbouring cavities which leads to more energy absorption in the marrow. Therefore, the TBVF of the MASH2 femur was increased to 37% by systematically and uniformly changing marrow voxels next to trabecular bone voxels into bone voxels throughout the μCT image until the desired TBVF was reached. Now the MASH2 AF(AM←AM) and the UF AF(AM←AM), both with 37% TBVF, agree within a margin of 1.6% on the average, showing a maximum difference of 6.4% at 1 MeV. The comparison with the UF data has shown that the application of similar dosimetric methods does not guarantee good agreement between the results, if one neglects the fact that apart from the cellularities, also the TBVFs should be similar.

3.3.3 Comparison with OLINDA

OLINDA/EXM (Stabin et al 2005) is a widely used computer software program for internal dose assessment in nuclear medicine, which calculates AFs and S-values for most standard organs based on the specific absorbed fractions (SAFs) derived for the adult, pediatric and pregnant female ORNL mathematical phantom series and on the skeletal AFs described in the paper of Stabin et al. (2002).

Table 14. S-values for the active marrow (AM) and the bone endosteum (BE) of the MASH2 skeleton for six radionuclides distributed homogeneously in the AM, on the trabecular bone surface (TBS) and in the trabecular bone volume (TBV). For comparison, the corresponding data given by the OLINDA software are also shown as well as the ratios S_M / S_O between the MASH2 and the OLINDA S-Values. BE thickness = 10 μm.

Radionuclide	Mean Beta Energy (MeV)	MASH2 S(AM←AM) (mGy/MBq-s)	OLINDA S(AM←AM) (mGy/MBq-s)	***RATIO*** S_M / S_O	MASH2 S(BE←AM) (mGy/MBq-s)	OLINDA S(BE←AM) (mGy/MBq-s)	***RATIO*** S_M / S_O
C-14	0.050	5.13E-06	5.18E-06	***0.989***	1.75E-06	2.06E-06	***0.850***
Fe-59*	0.118	1.20E-05	1.36E-05	***0.885***	4.99E-06	6.39E-06	***0.781***
I-131*	0.192	1.40E-05	1.55E-05	***0.903***	5.95E-06	8.20E-06	***0.726***
Sr-89	0.585	3.60E-05	3.75E-05	***0.960***	1.70E-05	2.31E-05	***0.738***
P-32	0.695	4.18E-05	4.42E-05	***0.945***	2.02E-05	2.75E-05	***0.733***
Y-90	0.933	5.32E-05	5.87E-05	***0.906***	2.59E-05	3.72E-05	***0.697***
Average				***0.931***			***0.754***
	Energy (MeV)	S(AM←TBS) (mGy/MBq-s)	S(AM←TBS) (mGy/MBq-s)	S_M / S_O	S(BE←TBS) (mGy/MBq-s)	S(BE←TBS) (mGy/MBq-s)	S_M / S_O
C-14	0.050	1.34E-06	1.50E-06	***0.893***	1.58E-05	1.57E-05	***1.004***
Fe-59*	0.118	4.56E-06	5.16E-06	***0.884***	1.75E-05	1.65E-05	***1.061***
I-131*	0.192	5.48E-06	6.91E-06	***0.793***	1.76E-05	1.83E-05	***0.962***
Sr-89	0.585	1.70E-05	2.35E-05	***0.724***	2.79E-05	2.80E-05	***0.997***
P-32	0.695	2.00E-05	2.82E-05	***0.708***	3.12E-05	3.22E-05	***0.968***
Y-90	0.933	2.60E-05	3.84E-05	***0.677***	3.85E-05	4.10E-05	***0.940***
Average				***0.780***			***0.989***
	Energy (MeV)	S(AM←TBV) (mGy/MBq-s)	S(AM←TBV) (mGy/MBq-s)	S_M / S_O	S(BE←TBV) (mGy/MBq-s)	S(BE←TBV) (mGy/MBq-s)	S_M / S_O
C-14	0.050	2.72E-07	1.67E-07	***1.628***	2.22E-06	2.18E-06	***1.019***
Fe-59*	0.118	3.17E-06	3.51E-06	***0.903***	6.91E-06	8.83E-06	***0.783***
I-131*	0.192	4.04E-06	5.08E-06	***0.795***	8.40E-06	1.05E-05	***0.800***
Sr-89	0.585	1.61E-05	2.18E-05	***0.736***	2.28E-05	2.34E-05	***0.975***
P-32	0.695	1.90E-05	2.65E-05	***0.717***	2.67E-05	2.76E-05	***0.968***
Y-90	0.933	2.51E-05	3.66E-05	***0.685***	3.41E-05	3.64E-05	***0.936***
Average				***0.911***			***0.913***

* includes also the gamma component

Table 14 presents a comparison between S-values of this study and of the OLINDA code in the AM and in the BE for electron-emitting radionuclides ^{14}C, ^{59}Fe, ^{131}I, ^{89}Sr, ^{32}P and ^{90}Y homogeneously distributed in the AM, the TBS and the TBV. The OLINDA data have been provided by M. Stabin (2010). The skeletal AFs used by the OLINDA code had been calculated with a 10 µm BE thickness. Therefore, the same thickness was used for the MASH2 skeleton. Although a revised version, the skeletal dosimetry of OLINDA is based on the data by Eckerman and Stabin already discussed in section 3.3.1. There, differences for mono-energetic AFs between 5 and 17% were found. In table 14, most average differences between the two skeletal dosimetry models are below 10%, except for the S(BE←AM) and for the S(AM←TBS) with average differences of 24.6 and 22%, respectively. The two techniques compared here actually differ with respect to all components of the skeletal dosimetry models used: the skeletons, the trabecular bone materials and the MC methods. Taking these differences into account, one can consider the comparison with the OLINDA S-values to be satisfactory.

3.4 Comparison with previous definitions of the endosteum

How does the change of the definition of the endosteum affect the absorbed dose to the osteogenic precursor cells? In order to answer this question, BE specific absorbed fractions (SAFs) of energy have been calculated for the ICRP, the Leeds and the UF model of the endosteum for the source regions TM and TBV, because SAFs, which are AFs divided by the mass of the target tissue, are proportional to the absorbed dose to the target tissue.

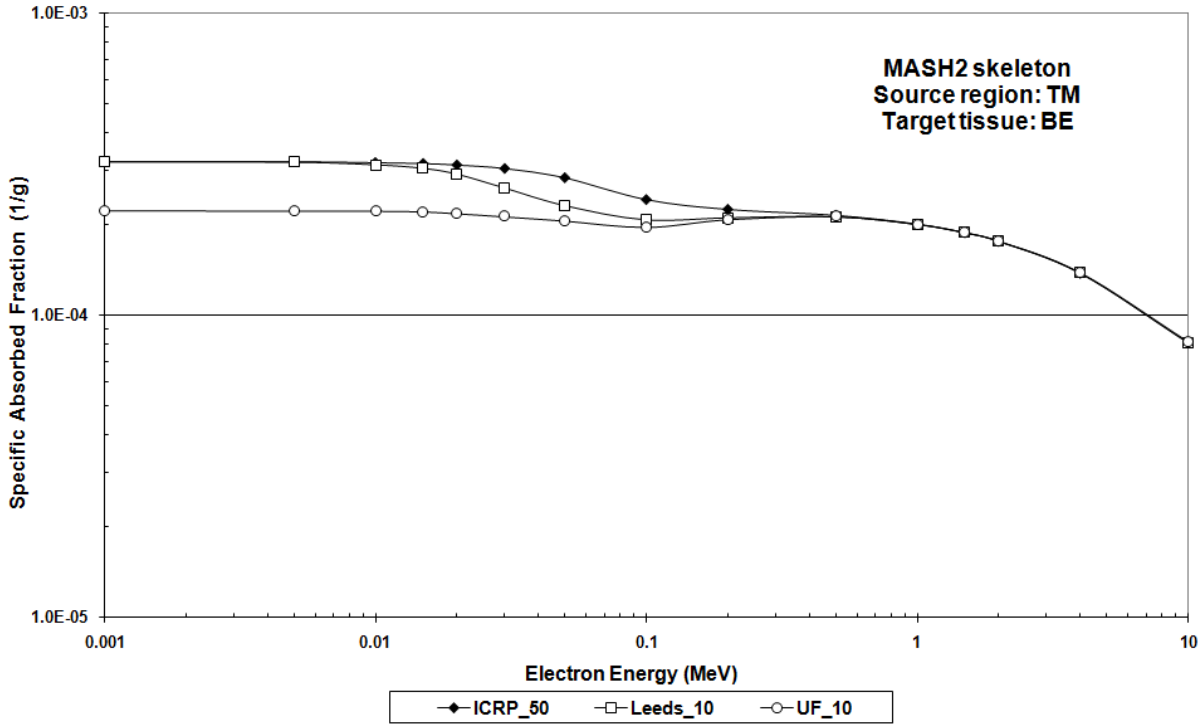

Figure 14. Specific absorbed fractions of energy in the bone endosteum (BE) for electrons isotropically emitted in the trabecular marrow (TM) as a function of the electron source energy for the following endosteum definitions: 50 µm ICRP model, 10 µm Leeds model and 10 µm UF model.

The 8 SP cluster method calculated the endosteum mass in the MASH2 skeleton for 10 µm thickness as 122 g, which is close to the reference value of 120 g recommended by ICRP30 (ICRP 1979). According to table 1, the BE mass for the 50 µm endosteum is 458.1 g. The ICRP and the Leeds model differ with respect to the thickness of the endosteum, however, both models consider the

endosteum to be a part of the marrow, i.e. when TM is the source region, electrons are also emitted in the endosteum volume. For all three models, figure 14 shows SAF(BE←TM) as a function of the electron energy between 1 keV and 10 MeV. For incident electron energies up to 10 keV, the ICRP and the Leeds SAFs are equal, because, according to table 2, the CSDA ranges of the emitted particles are less than 2.5 µm, which actually represents self-irradiation of both endostei. With increasing energy and therefore increasing range, relatively more electrons leave the 10 µm layer than the 50 µm layer to deposit energy in bone or marrow which explains why the Leeds SAF is up to 23% (at 50 keV) smaller than the ICRP SAF. At the same time, electrons coming from other parts of the TM increasingly deposit energy in the 50 µm and then also in the 10 µm layer, which becomes the dominant source of homogeneous energy deposition in both endostei. Therefore, above 500 keV, both SAFs become equal again. In the UF model, the endosteum is not part of the marrow and consequently here not part of the source region. Therefore, and because of the smaller endosteum thickness, the UF SAF is 45% smaller than the ICRP SAF for electron energies up to 30 keV. With further increasing energy the UF SAF approaches the SAFs for the other endosteum models at about 500 keV.

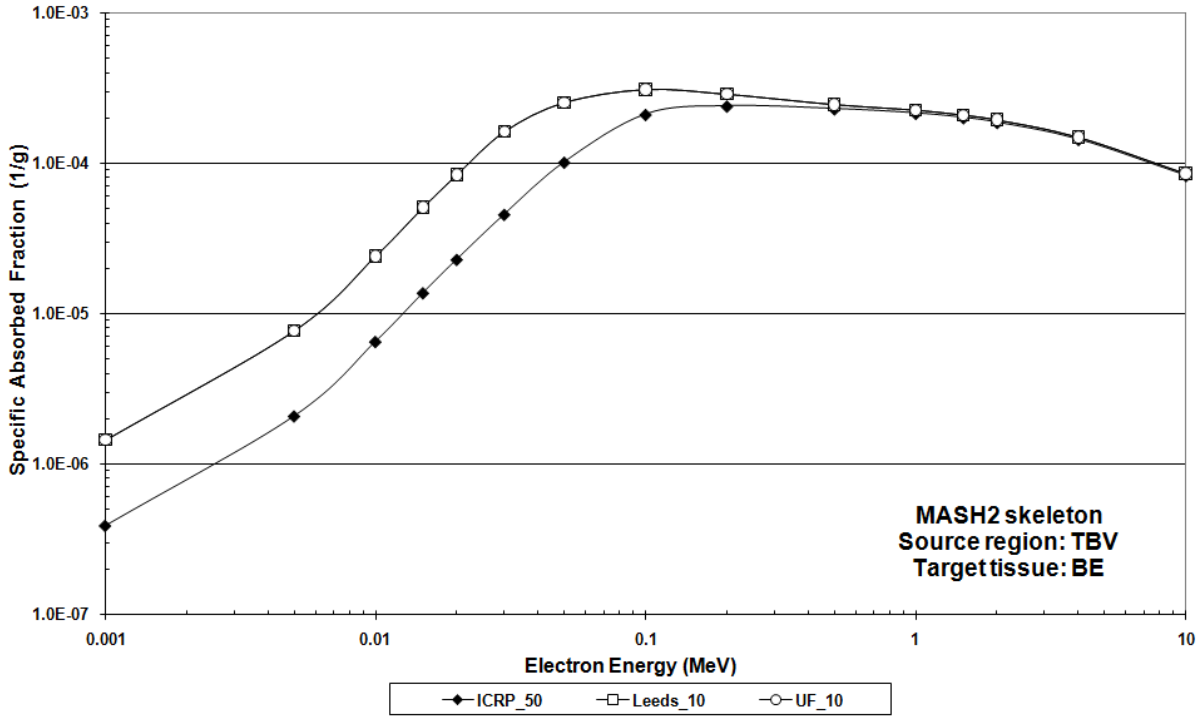

Figure 15. Specific absorbed fractions of energy in the bone endosteum (BE) for electrons isotropically emitted in the trabecular bone volume (TBV) as a function of the electron source energy for the following endosteum definitions: 50 µm ICRP model, 10 µm Leeds model and 10 µm UF model.

Figure 15 shows SAF(BE←TBV) as a function of the electron energy again for all three endosteum models. The Leeds and the UF SAFs are equal because when the source is located outside the marrow, here in trabecular bone, it does not matter for the value of the SAF(BE←TBV) if the endosteum is considered to be part of the marrow or not. While for the TM source, presented in figure 14, only a moderate change of about 20% for the SAF(BE←TM) was found, figure 15 shows a quite different situation for the TBV source. Increasing the endosteum thickness from 10 to 50 µm causes a decrease of the SAF(BE←TBV) by a factor of 3.7 for electron energies up to 30 keV. With further increasing energy the difference becomes smaller, showing factors of 2.5, 1.5 and 1.2 at 50, 100 and

200 keV, respectively. Above 500 keV the difference drops to a few percent. Electrons released in bone, entering the marrow cavities deposit energy in the marrow as a function of their energy, i.e. as a function of the penetration depth into the cavity. Consequently, a 10 μm layer on the bone surface receives a greater SAF or absorbed dose than a 50 μm layer, unless the energy is high enough to guarantee homogeneous irradiation through both layers. This phenomenon has also been discussed for photoelectrons released in bone by external photon irradiation (Kramer et al 2007). Notwithstanding the results for other source/target combinations, the data suggest that for TBV, TBS, CBV and CBS sources, the increase of the endosteum thickness from 10 to 50 μm leads to a significant decrease of the average endosteum absorbed dose for energies up to 100 keV, while for AM, IM and TM sources the average endosteum absorbed dose changes only moderately, at least compared to the Leeds model. Similar data for the target tissue AM show differences smaller than 1% and 6% for ICRP versus Leeds and for ICRP versus UF, respectively, for the TM source and smaller than 1% for all comparisons for the TBV source.

4. Conclusions

The recently developed 8 SP cluster method for skeletal dosimetry has been applied to external exposure to photons. This study extended the application of the method to internal exposure from bone-seeking radionuclides, especially those emitting electrons. The calculations of AFs and S-values in the AM and the BE have been undertaken in the skeleton of the MASH2 phantom based on μCT images of trabecular bone. The ICRP110 concept of skeletal tissue regions was used for the modeling of the BE layer thickness and the AM. Eight skeletal source regions have been considered in the calculations and, apart from the AM and the BE, AFs were also calculated for organs and tissues located outside the skeleton. Corresponding data calculated in the female FASH2 phantom produced results very similar to those for the male MASH phantom. Therefore, the study was restricted to the presentation of the male adult results.

It seems that currently there are no similar data available from other investigations using the ICRP110 concept for skeletal dosimetry. Therefore, the 8 SP cluster method was modified with respect to the BE layer thickness and to the modelling of skeletal regions in order to make comparisons with data from others possible. These comparisons turned out to be satisfactory if one takes the methodological differences of the skeletal dosimetry models used into account. Comparison with previous definitions of the endosteum indicate that the increase of the thickness from 10 to 50 μm leads to a significant decrease of the average endosteum absorbed dose in the low energy range especially for electron sources concentrated in bone, while the effect on the average endosteum absorbed dose is only moderate for soft tissue sources in the marrow cavities.

The microstructure of spongiosa was first introduced into skeletal dosimetry by Spiers and co-workers from the University of Leeds/England by using 2-dimensional chord length distributions through trabeculae and cavities measured in human bone samples. The group of W. Bolch from the University of Florida extended this approach to a 3-dimensional representation of the microstructure based on μCT images of trabecular bone for specific bone sites. The 8 SP cluster method as described in this and earlier papers of the computational dosimetry group of the Department of Nuclear Energy at the UFPE extended the 3-dimensional approach to the complete skeletons of anthropomorphic human phantoms. To our knowledge, MASH and FASH are currently the only human phantoms "equipped" with trabecular microstructure in their skeletons and connected to a Monte Carlo code which segments AM, IM and BE in all spongiosa voxels at runtime and calculates AFs, SAFs, S-values and organ and tissue equivalent doses for skeletal tissues for external and internal exposure to photons and electrons. The MASH and the FASH phantoms as well as the micro matrices for the spongiosa voxels are available on www.caldose.org.

Although quite sophisticated, the 8 SP cluster method represents just another milestone during the process of steadily improving skeletal dosimetry. This paper assumed quiescent bone surfaces, which is a reasonable first approximation for the adult skeleton. However, forming bone surfaces and various physiological processes may influence uptake, retention and clearance of radionuclides and associated cancer risks, especially in the paediatric skeleton (Richardson 2010). Consequently, further development of the 8 SP cluster method would have to take such physiological processes into account.

5. Acknowledgements

The authors would like to thank the Conselho Nacional de Desenvolvimento Científico e Tecnológico - CNPq and the Fundação de Amparo à Ciência do Estado de Pernambuco - FACEPE for financial support and Prof. M G Stabin for providing the OLINDA AFs shown in the comparison in section 3.3.3.

6. References

Beddoe A H, Darley P J and Spiers F W 1976 Measurements of Trabecular Bone Structure in Man Phys Med Biol **21** 4 589-607

Bolch W E, Patton P W, Rajon D A, Shah A P, Jokisch D W and Inglis B A 2002 Considerations of Marrow Cellularity in the 3-Dimensional Dosimatric Models of the Trabecular Skeleton *J Nucl Med* **43:**97- 108

Bolch W E, Shah A P, Watchman C J, Jokisch D W, Patton P W, Rajon D A, Zankl M, Petoussi-Henss N and Eckerman K F 2007 Skeletal Absorbed Fractions for Electrons in the Adult Male: Considerations of a Revised 50-μm Definition of the Bone Endosteum *Rad.Prot.Dos*. **127** 169-173

Bouchet L G, Jokisch D W and Bolch W E 1999 A Three-Dimensional Transport Model for Determining Absorbed Fractions of Energy for Electrons Within Trabecular Bone J Nucl Med **40:**1947-1966

Bouchet L G, Bolch W E, Howell R W and Rao D V 2000 S Values for Radionuclides Localized Within the Skeleton J Nucl Med **41:**189-212

Cassola V F, de Melo Lima V J, Kramer R and Khoury H J 2010a FASH and MASH: Female and Male Adult human phantoms based on polygon meSH surfaces. Part I: Development of the anatomy *Phys Med Biol* **55** 133-162

Cassola V F, Kramer R, Brayner C and Khoury H J 2010b Poster-specific phantoms representing female and male adults in Monte Carlo-based simulations for radiological protection *Phys Med Biol* **55** 4399-4430

Cristy M 1981 Active bone marrow distribution as a function of age in humans Phys Med Biol **26** 3 389-400

Cristy M and Eckerman K F 1987 Dose-Response Functions for soft tissues of the skeleton In: Specific Absorbed Fractions of Energy at Various Ages from Internal Photon Sources. I. Methods *ORNL/TM-8381/V1* Oak Ridge National Laboratory, TN, USA

Eckerman K F 1985 Aspects of the dosimetry of radionuclides within the skeleton with particular emphasis on the active marrow Proceedings of the Fourth International Radiopharmaceutical Dosimetry Symposium, 1985, Oak Ridge, TN, ORAU, CONF-85113 514-534

Eckerman K F and Stabin M G 2000 Electron Absorbed Fractions and Dose Conversions Factors for Marrow and Bone by Skeletal Regions *Health Phys.* **78** 2 199-214

ICRP 1979 Limits for Intakes of Radionuclides by Workers *ICRP Publication 30* (Oxford: Pergamon)

ICRP 1995 Basic Anatomical and Physiological Data for use in Radiological Protection: The Skeleton. ICRP Publication 70 *(Oxford: Pergamon)*

ICRP 2002 Basic Anatomical and Physiological Data for Use in Radiological Protection: Reference Values ICRP Publication 89 *(Oxford: Pergamon)*

ICRP 2008Nuclear Decay Data for Dosimetric Calculations ICRP Publication 107 *(Oxford: Pergamon Press)*

ICRP 2009 Adult Reference Computational Phantoms ICRP Publication 110 *(Oxford: Pergamon)*

ICRU 1992 Photon, Electron, Proton and Neutron Interaction Data for Body Tissues *ICRU Report No. 46* International Commission On Radiation Units And Measurements, Bethesda, MD, USA

Jokisch D W, Bouchet L G, Patton P W, Rajon D A and Bolch W E 2001 Beta-particle dosimetry of the trabecular skeleton using Monte Carlo transport within 3D digital images *Med.Phys.* **28** (7), 1505-1518

Kawrakow I and Rogers D.W.O. 2003 The EGSnrc code system: Monte Carlo simulation of electron and photon transport, *NRC Report PIRS-701*

King S D, Spiers F W 1985 Photoelectron enhancement of the absorbed dose from X rays to human bone marrow: experimental and theoretical studies Br. J. of Radiol. **58** 345-356

Kramer R 1979 Determination of conversion factors between organ equivalent doses and operational quantities for external exposure to X- and gamma rays, Gesellschaft fuer Strahlen-und Umweltforschung, Muenchen-Neuherberg, GSF-Bericht-S-556

Kramer R, Vieira J W, Khoury H J, Lima F R A and Fuelle D 2003 All About MAX: a Male Adult voXel Phantom for Monte Carlo Calculations in Radiation Protection Dosimetry *Phys Med Biol* **48** 10 1239-1262

Kramer R, Vieira J W, Khoury H J, Lima F R A, Loureiro E C M, Lima V J M and Hoff G 2004 All about FAX: a Female Adult voXel Phantom for Monte Carlo Calculation in Radiation Protection Dosimetry, Phys. Med. Biol. **49**, 5203-5216

Kramer R, Khoury H J, Vieira J W and Lima V J M 2006a MAX06 and FAX06: Update of two adult human phantoms for radiation protection dosimetry *Phys. Med. Biol.* **51** 3331-3346

Kramer R, Khoury H J, Vieira J W and Kawrakow I 2006b Skeletal dosimetry in the MAX06 and the FAX06 phantoms for external exposure to photons based on vertebral 3D-microCT images *Phys.Med.Biol.* **51** 6265-6289

Kramer R, Khoury H J, Vieira J W and Kawrakow I 2007 Skeletal dosimetry for external exposure to photons based on μCT images of spongiosa from different bone sites *Phys.Med.Biol. **52** 6697-6716*

Kramer R, Khoury H J, Vieira J W and Robson Brown K A 2009a Skeletal dosimetry for external exposures to photons based on μCT images of spongiosa: Consideration of voxel resolution, cluster size and medullary bone surfaces Med Phys **36** 11 5007-5016

Kramer R, Khoury H J, Vieira J W, Robson-Brown K and Fuelle D 2009b Electron absorbed fractions in skeletal soft tissues based on red bone marrow segmentation at runtime in microCT images of human trabecular bone *World Congress 2009 – Medical Physics and Biomedical Engineering, 7-12 September 2009, Munich, Germany.*

Kramer R, Cassola V F, Khoury H J, Vieira J W, de Melo Lima V J and Robson Brown K 2010 FASH and MASH: female and male adult human phantoms based on polygon mesh surfaces: II. Dosimetric calculations, *Phys Med Biol* **55** 163-189

Nie H and Richardson R B 2009 Radiation dose to trabecular bone marrow stem cells from ^{3}H, ^{14}C and selected α-emitters incorporated in a bone remodeling compartment Phys Med Biol **54** 963-979

Richardson R B and Dubeau J 2003 Monte Carlo determination of age-dependent steady-state dose to red bone marrow and bone from ^{14}C exposure *Radiat. Prot. Dosim.* **103** No.1 5-18

Richardson R B, Nie H L and Chettle D R 2007 Monte Carlo Simulation of Trabecular Bone Remodeling and Absorbed Dose Coefficients for Tritium and ^{14}C Rad Prot Dos **127** 1-4 158-162

Richardson R B 2010 A physiological skeletal model for radionuclide and stable element biokinetics in children and adults *Health Phys* **99** 4 471-482

Rosenstein M 1976 Organ Doses in Diagnostic Radiology US Department of Health, Education and Welfare, Bureau of Radiological Health BRH Tech. Publ. DA 76-8030

Schlattl H, Zankl M and Petoussi-Henss N 2007 Organ dose conversion coefficients for voxel models of the reference male and female from idealized photon exposures *Phys Med Biol* ***52*** *2123-2145*
Shah A P, Bolch W E, Rajon D A, Patton P W and Jokisch D W 2005a A Paired-Image Radiation Transport Model for Skeletal Dosimetry *J Nucl Med* **46**, No.2, 344-353
Shah A P, Rajon D A, Patton P W, Jokisch D W and Bolch W E 2005b Accounting for beta-particle loss to cortical bone via paired-image radiation transport (PIRT) *Med.Phys.* **32** (5), 1354-1366
Spiers F W 1949 The influence of energy absorption and electron range on dosage in irradiated bone Br J Radiol **22** 261 521-533
Spiers F W 1969 Transition-Zone Dosimetry *Radiation Dosimetry* Second Edition, Volume III, Sources, Fields, Measurements and Applications, Academic Press, New York and London
Spiers F W 1963 Interim Report on the determination of dose to bone marrow from radiological procedures Br. J. of Radiol. **36** 424 238-240
Spiers F W 1968 Radioisotopes in the Human Body, Academic Press
Spiers F W 1974 Radionuclides and bone – from ^{226}Ra to ^{90}Sr *Br.J.Radiol.* **47** 564, 833-844
Spiers F W, Beddoe A H and Whitwell J R 1978 Mean skeletal dose factors for beta-particle emitters in human bone. Part I: volume-seeking radionuclides Br J Radiol **51** 622-627
Spiers F W, Beddoe A H and Whitwell J R 1981 Mean skeletal dose factors for beta-particle emitters in human bone. Part II: surface-seeking radionuclides Br J Radiol **54** 500-504
Spiers F W 1988 Particle dosimetry in bone and the toxicity of bone-seeking radionuclides Phys Med Biol **33** 4 395-411
Stabin M G 1996 MIRDOSE – the personal computer software for use in internal dose assessment in nuclear medicine J Nucl Med **37:**538-546
Stabin M G, Eckerman K F, Bolch W E, Bouchet L G and Patton P W 2002 Evolution and Status of Bone and Marrow Dose Models Cancer Biotherapy & Radiopharamaceuticals **17** 4 427-433
Stabin M G, Sparks R B and Crowe E 2005 OLINDA/EXM: The Second-Generation Personal Computer Software for Internal Dose Assessment in Nuclear Medicine J Nucl Med **46:** 1023-1027
Stabin M G personal communication per email on October 26, 2010
Watchman C J, Hasenauer D and Bolch W E 2007 Derivation of site-specific skeletal masses within the current ICRP age series, *Phys Med Biol* **52** 3133-3150
Whitwell J R and Spiers F W 1976 Calculated Beta-ray Dose Factors for Trabecular Bone Phys Med Biol **21** 1 16-38